Adaptation of redox metabolism in drug-tolerant persister cells is a vulnerability to prevent relapse in pancreatic cancer

Nadine Abdel Hadi[1], Gabriela Reyes-Castellanos[1], Tristan Gicquel[1], Scarlett Gallardo-Arriaga[1], Emeline Boet[2], Jean-Emmanuel Sarry[2], Rawand Masoud[1], Juan Iovanna[1], Alice Carrier[1,*]

Affiliations:

[1]Aix Marseille Univ, Inserm, CNRS, Institut Paoli-Calmettes, Centre de Recherche en Cancérologie de Marseille (CRCM), Marseille, France.

[2]Centre de Recherches en Cancérologie de Toulouse, Université de Toulouse, Inserm, CNRS, Toulouse, France.

*To whom correspondence should be addressed: Alice Carrier, Centre de Recherche en Cancérologie de Marseille (CRCM), Campus de Luminy Case 915, 163 Avenue de Luminy, 13288 Marseille Cedex 9, France. Phone: +33 491828829; Fax: +33 491826083. Email: alice.carrier@inserm.fr.

ABSTRACT

Objective Pancreatic Ductal Adenocarcinoma (PDAC) remains a major unresolved disease because of its remarkable therapeutic resistance. Even patients who respond to initial therapy experience relapse in most cases. The mechanisms underlying therapy-acquired resistance supporting relapse are poorly understood. In this study, we explored metabolic vulnerabilities of PDAC tumors during relapse, specifically adaptations of mitochondrial and redox metabolism.

Design We used preclinical PDAC mouse models that respond to chemotherapeutic treatment but relapse after complete regression: heterotopic (subcutaneous) patient-derived xenografts, and orthotopic syngeneic allografts. Relapsed tumors were analyzed *ex vivo* by flow cytometry to measure mitochondrial and redox characteristics. Total ATP level and molecular mechanisms underlying the reprogramming were determined.

Results Mitochondrial metabolism is reprogrammed during relapse, with increased mitochondrial mass, ATP levels, mitochondrial superoxide anions and total ROS levels in relapsed compared to control tumors in both models; mitochondrial membrane potential is increased in the xenografts model only. This mitochondrial metabolic reprogramming occurs during treatment-induced regression and at the onset of relapse. At the molecular level, antioxidant defenses were found to be increased in relapsed tumors and during treatment. These data suggest that treatment-induced oxidative stress may cause the appearance of treatment-adapted cells, also known as residual or persister cells. Finally, we found that the combined treatment of arsenic trioxide (ROS inducer) and buthionine sulfoximine (glutathione synthesis inhibitor) was able to completely prevent relapse in PDAC xenografts.

Conclusion Targeting redox metabolism via promoting ROS production and inhibiting antioxidant capacity is a very promising approach to prevent relapse in PDAC patients.

Keywords: Pancreatic cancer; relapse; mitochondrial metabolism; ROS; oxidative stress; targeted therapy.

Significance of this study

What is already known on this subject?

- Pancreatic ductal adenocarcinoma (PDAC), the most common form of pancreatic cancer, is the fourth leading cause of cancer-related death in the Western world and is predicted to become the second by 2030.
- Most of the patients experience resistance to treatment and develop disease recurrence at some point during treatment or after remission.
- PDAC tumors that show an oxidative phenotype are dependent on mitochondrial metabolism, supporting a role for mitochondria in primary PDAC resistance.
- A pro-survival role of mitochondria in pancreatic cancer stem cells (or dormant cells) has been reported.

What this study adds?

- Our study shows that the mitochondrial metabolism is reprogrammed during relapse, with increased mitochondrial mass, ATP levels, and mitochondrial superoxide anions and total ROS levels in relapsed tumors in both xenograft and allograft models.
- The reprogramming of mitochondrial and redox metabolism occurs during treatment-induced regression and at the onset of relapse, supporting the survival of treatment-adapted cells also known as residual or persister cells.
- Post-treatment with oxidizing agents was able to completely prevent relapse in PDAC xenografts.

How might it impact on clinical practice in the foreseeable future?

- This study is opening new avenues for better therapeutic management of PDAC patients in the clinic.

INTRODUCTION

The pancreatic ductal adenocarcinoma (PDAC) is the most common cancer of the pancreas. To date, it is the fourth leading cause of cancer-related death in the Western world and is predicted to become the second leading cause of cancer death in the United States by 2030 [1–3]. PDAC remains an incurable disease, with the lowest 5-year survival rate after diagnosis at only 10% [3,4]. This situation reflects the slow progress against this disease due to a lack of early diagnosis and major treatment advances. The poor prognosis of PDAC is linked to a high percentage of locally advanced or metastatic diseases at the time of diagnosis, and the limited effectiveness of anti-tumor treatments, including immunotherapies [5,6]. A small proportion of patients (less than 20%) show a localized tumor eligible for resection at diagnosis. Surgery followed by chemotherapy increases the median survival from 6 to 21 months, but most of the patient experience resistance to treatment and develop disease recurrence at some point during treatment or after remission. It is therefore imperative to identify more effective therapies against this dreadful disease.

Oncologists are confronted with two types of resistance to therapy: primary resistance is non-response to conventional treatments, while acquired resistance (therapy-induced resistance) is relapse (recurrence) after an initial response to therapy [7]. The common mechanisms involved in chemoresistance include an alteration of drug metabolism, changes in drug targets, apoptosis suppression, activation of intracellular survival signaling, enhanced DNA damage repair, epithelial-mesenchymal transition (EMT), immune escape of cancer stem cells, epigenetic alteration, and aberrant metabolism [8]. Regarding acquired resistance, a major role has recently been suggested for a subpopulation of drug-tolerant cells present in cancer populations, called “persistent” or "persister" cells, which survive drug treatment and regain their proliferative capacity, through different strategies [9]. A common feature of many persister cancer cells is the adaptation of cellular metabolism, particularly increased mitochondrial oxidative metabolism, which has been demonstrated in different types of cancers [10–14]. Another metabolic characteristic of persistent cells is the overproduction of reactive oxygen species (ROS) and the increase of antioxidant defenses to counteract the overproduction of ROS, allowing cell survival. Such a process includes the increase in glutathione levels, which is commonly observed in various persister

cancer cells [15–17]. In addition, phospholipid glutathione peroxidase 4 (GPX4) activity has been shown to increase in drug persister from human breast cancer, lung cancer, melanoma cells and colorectal cancer [16,18,19].

Interestingly, in pancreatic cancer, tumors showing an oxidative phenotype are dependent on mitochondrial metabolism, supporting a role for mitochondria in primary PDAC resistance [20–24]. A pro-survival role of mitochondria in pancreatic cancer stem cells (or dormant cells) has been reported [25–28]. However, the role of mitochondrial metabolism in acquired resistance during PDAC therapeutic treatment remains poorly explored. We found in our laboratory that inhibiting mitochondrial fatty acid oxidation (FAO) in combination with chemotherapy induces complete xenograft regression for a subset of PDAC patients. Strikingly, we observed that all residual tumors relapse after a period of time, mirroring what happens in patients. In the study presented here, we explored mitochondrial metabolic adaptations in PDAC tumors during relapse, in particular adaptations in redox metabolism. This study was conducted exclusively *in vivo* using our preclinical mouse models (patient-derived xenografts and syngeneic allografts) that relapse after chemotherapy-induced regression.

MATERIALS AND METHODS

Animal models

Xenograft mouse models of Pancreatic Ductal AdenoCarcinoma (PDAC)

We performed subcutaneous xenografts in immunodeficient mice using two different primary human PDAC cells, as described in Reyes-Castellanos et al. (in revision). Recipient mice were 5- to 6-week-old athymic female, Swiss nude mice, SOPF (Specific and Opportunistic Pathogen Free) health status, strain Crl:Nu(lco)-Foxn1^{nu} (Charles River, France). To obtain the xenografts, the subcutaneous tumor from an initial mouse donor was removed and finely minced with a scalpel. Then, 150 mg of tumor's pieces were mixed with 50 µL of Matrigel and implanted with a trocar (10 Gauge) in the subcutaneous space of recipient isoflurane-anesthetized mice. Tumor volume was measured twice per week using a digital caliper and tumor volume was calculated with the formula V = length x (width)^2/2.

When xenografts reached ~ 200 mm^3 volume, mice were randomly assigned in a treatment group in which the average of all tumors was 200 mm^3. Treatments were administered by intraperitoneal injection during one month as follows: Gemcitabine 120 mg/kg intraperitoneally (IP) twice a week, or Gemcitabine plus Perhexiline (120 mg/kg IP twice a week and 5 mg/kg IP every other day, respectively). Vehicle-injected mice (controls) were injected with PBS in the case of Gemcitabine controls or 3% DMSO in PBS for combination treatment controls. Mice whose tumor volume reached 1.5 cm^3 were ethically sacrificed and tumors removed.

The *in vivo* therapeutic effect of arsenic trioxide (ATO, AS_2O_3) and L-buthionine sulfoximine (BSO) was evaluated in the xenograft mouse model. Mice were divided into different groups (at least n=4 *per* condition): PBS (vehicle control), AS_2O_3 (5 mg/kg), and BSO (30 mg/kg). AS_2O_3 was administrated ÏP daily (5 days a week), starting right after the end of the one-month chemotherapy treatment inducing complete tumor regression, and during one, two or three months. BSO was administrated IP 3 times per week for 2 months; BSO treatment started with several days of delay (9 and 16 days for PDAC032T and PDAC084T xenografts, respectively) after the end of the one-month chemotherapy treatment.

Syngeneic allograft mouse model of Pancreatic Ductal AdenoCarcinoma (PDAC)

Orthotopic syngeneic allografts were generated by intraperitoneal injection of one million of the murine cells KPC luc2 into 6-week-old female C57BL/6 mice (immunocompetent strain, SOPF health status, Charles River, France). Tumoral growth was followed by bioluminescence upon injection of 3 mg luciferin-EF (Promega) using a Photon Imager device (Biospace Lab). Twelve days post-grafting, tumor-bearing mice were randomly assigned to two treatment cohorts (at least n = 5 per condition), vehicle control (treated with PBS) and Gemcitabine 120 mg/kg twice a week by intraperitoneal injection during one month. Mice were sacrificed according to the ethical limit point.

All mice were kept under specific pathogen-free conditions and according to the current European regulation; the experimental protocol was approved by the Institutional Animal Care and Use Committee (#16711).

Tumor dissociation

Xenograft and allograft tumors were dissociated using the gentle MACS™ Octo Dissociator with Heaters and the Tumor Dissociation Kit, mouse (130-096-730), as per manufacturer's instructions. Briefly, tumors were cut into small pieces of 2-4 mm and resuspended in RPMI 1640 media supplemented with 2% FBS (Thermo Scientific, Waltham, MA, USA). These pieces then underwent mechanical and enzymatic digestion for 1 hour. Immediately following dissociation, all single-cell suspensions were filtered using a MACS SmartStrainer (70 µm). The suspensions were centrifuged for 7 min at 300 g at room temperature, the supernatant aspirated, and the cells were resuspended in RPMI 2% FBS media. Cells were counted by flow cytometry using MACSQuant-VYB (Miltenyi Biotec).

Flow cytometry *ex vivo*

Mitochondrial mass and mitochondrial membrane potential measurements

Mitochondrial mass and mitochondrial membrane potential measurements were performed using MitoTracker Deep Red (M22426), and the MitoProbe™ TMRM Kit

(M20036), respectively. Briefly, 200,000 cells were collected after tumor dissociation, centrifuged and labeled with MitoTracker and TMRM to a final concentration of 200 nM and 20 nM for 10 min and 30 min, respectively. Then, 10,000 events per sample were acquired in a MACSQuant-VYB (Miltenyi Biotec), and data analysis was performed using the FlowJo software.

Total ROS and mitochondrial superoxide anions detection

Total ROS and mitochondrial superoxide anions measurements were performed using CellRox Orange (C-10443), and MitoSOX Red (M36008), respectively. Briefly, after tumor dissociation, 200,000 cells were collected, centrifuged and labeled with CellROX and MitoSOX to a final concentration of 5µM and 10 µM for 30 min and 20 min, respectively. After incubation, cells were centrifuged, and resuspended in PBS 1x for flow cytometry analysis. 10,000 events per sample were acquired in a MACSQuant-VYB (Miltenyi Biotec), and data analysis was performed using the FlowJo software.

Measurement of total, mitochondrial and glycolytic ATP

Total ATP levels were measured using the Cell viability assay (Cell-Titer Glo Kit; Promega) according to the manufacturer's instructions. Briefly, 50,000 cells were resuspended in 100 µL of medium and distributed in four replicates in a 96-well flat-bottom plate. Cells were then treated with PBS (Control), 1µM oligomycin (inhibitor of mitochondrial respiration), and 100mM 2-DG (inhibitor of glycolysis). Following one hour of incubation at 37ºC, 100 µL of Cell Titer Glo reaction mix solution was added to each well for a final volume of 200 µL. Plates were then analyzed by luminescence using Tristar LB 941 apparatus (Berthold technologies). The background relative light unit (RLU) was subtracted from each RLU value. By comparing the different conditions, total ATP (PBS condition) and percentages of both mitochondrial and glycolytic ATP were determined: mitochondrial ATP = Total ATP - ATP (oligomycine); mitochondrial ATP (%) = mitochondrial ATP / Total ATP *100; glycolytic ATP = Total ATP - ATP (2DG); glycolytic ATP (%) = glycolytic ATP / Total ATP *100.

Quantification of small antioxidant molecules

GSH/GSSG measurement

GSH/GSSG-Glo Assay kit (Promega, V6611) was used following manufacturer's protocol with some modifications. Briefly, 10 mg of tumor tissue were crushed using Precellys® Evolution, resuspended in 50 µL of PBS/EDTA and distributed in a 96 well plate. After homogenization, 50µl of Total Glutathione Lysis Reagent (for Total glutathione measurement) and Oxidized Glutathione Lysis Reagent (for GSSG measurement) were added. Luciferin Generation Reagent and Detection Reagent were added to all wells and luminescence was recorded using Tristar LB 941 apparatus (Berthold technologies). By comparing the different conditions, GSH/GSSG ratio was calculated using the following equation: GSH/GSSG = (total glutathione RLU - GSSG RLU) / (GSSG RLU/2).

NADPH measurement

10 mg of tumor tissue were crushed using Precellys® Evolution, resuspended in 50 µL of PBS/EDTA, and distributed in a 96 well plate. Measurement was performed according to the manufacturer's protocol. Briefly, 50 µl of NADP/NADPH-Glo™ Detection Reagent (Promega, G9081) was added to each well and incubated for 30 minutes at RT. Luminescence was recorded using Tristar LB 941 apparatus (Berthold technologies).

Gene expression analysis by RT-qPCR

RNA was extracted from PDAC tumors using the RNeasy Mini kit (Qiagen) according to manufacturer's instructions. Then, RNA samples were subjected to reverse-transcription (RT) using the Go Script reagent (Promega) following manufacturer's instructions. Next, Real-Time quantitative PCR was performed in triplicates using Takara reagents and the Stratagene cycler Mx3005P QPCR System. Raw values were normalized with the housekeeping gene TBP1 for the same cDNA sample. We used the human primers for NRF2, HO-1, SLC7a11, and GPX4 involved in the antioxidant defense, PGC-1α and TFAM involved in mitochondrial metabolism. Primer sequences can be found in (Huang C et al., 2021). For each RNA sample, RT reaction was done twice to generate 2 batches of cDNA, which were amplified by qPCR in three independent experiments for each gene.

In vitro assays

Cell viability

Cells were seeded in 96-well plates in triplicates (5,000 cells per well) and the day after, the corresponding treatment was administered. Cells were treated with Perhexiline (7 µM), Gemcitabine (1 µM) or the combination for 24 hours. These treatments were done in the presence and the absence of NAC (2.5 mM). Next, cell viability was determined by the Crystal violet viability assay, which is independent from cell metabolism. For this, cells were fixed in glutaraldehyde (1%), washed twice with PBS, stained with Crystal violet (0.1%) for 10 min, and then washed three times with PBS. Crystals were solubilized in SDS (1%), and absorbance was measured at 600 nm using an Epoch-Biotek spectrophotometer.

Total ROS measurement by flow cytometry

Cells were seeded in 12-well plates in duplicates (200,000 cells/1 ml media/well) and the day after, treatments were administered. Cells were treated with Perhexiline (7 µM), Gemcitabine (1 µM) or the combination for 24 hours. After treatments, the media was supplemented with CellROX Orange at a final concentration of 5 µM. Cells were incubated for 30 minutes at 37°C, then harvested with pre-warmed Accutase (Gibco) and resuspended in PBS for flow cytometry analysis. 10,000 events per sample were acquired in a MACSQuant-VYB (Miltenyi Biotec), and data analysis was done with the FlowJo software.

Statistical analysis

Results are expressed as the mean ± SEM or SD of duplicates or triplicates, and at least two or three independent experiments were done for each analysis. Statistical analysis of data was performed with GraphPad Prism 8 (GraphPad Software) using two-tailed unpaired Student's t-test. P values < 0.05 were considered to be statistically significant (*$P < 0.05$, **$P < 0.01$, ***$P < 0.001$, and ****$P < 0.0001$).

RESULTS

The mitochondrial metabolism is reprogrammed in relapsed PDAC tumors

We used two subcutaneous PDAC xenograft models, PDAC032T and PDAC084T xenografts, which always relapse after complete regression induced by the chemotherapy, namely gemcitabine alone or combined with perhexiline (FAO inhibitor) respectively (Figure 1A and B). We analyzed mitochondrial characteristics and ROS levels in relapsed tumors at the ethical end point. Flow cytometry data presented in Figure 1C (gating strategy presented in Supplementary Figure 1) illustrate that mitochondrial mass, mitochondrial membrane potential (MMP), mitochondrial superoxide anion ($O_2^{\cdot -}$) level, and total ROS level are higher in relapsed xenografts (in both models) compared with controls. Interestingly, only a portion of the increase in MMP and mitochondrial $O_2^{\cdot -}$ comes from the increase in mitochondrial mass, as shown in the normalized data (Supplementary Figure 2A). In addition, we found a higher level of total ATP in the relapsed PDAC084T xenograft, a higher percentage of ATP produced by mitochondria in both relapsed xenografts, and a higher percentage of ATP produced by glycolysis in the relapsed PDAC032T xenograft (Figure 1D and Supplementary Figure 2B), suggesting higher energy production in both settings.

Metabolic variations during relapse were also observed in an immunocompetent PDAC mouse model, namely syngeneic allografts (Figure 2). In this model, murine luciferase-expressing PDAC cells implanted into the peritoneal cavity of syngeneic recipient mice grow preferentially in the pancreas, thus providing a very convenient orthotopic allograft model in which tumor growth and regression can be monitored by bioluminescence *in vivo* (Figure 2B). All tumors respond to gemcitabine treatment and regress, either completely or partially, and then relapse during or after the end of the 1-month treatment (Figure 2B and C). Interestingly, mitochondrial mass and total ROS level are significantly higher in relapsed tumors compared to control only for tumors that have fully regressed. In contrast, mitochondrial $O_2^{\cdot -}$ level is higher in both settings. In contrast to the xenografts presented above, MMP is decreased in relapsed tumors compared to control. Only part of the increase in mitochondrial $O_2^{\cdot -}$ comes from the increase in mitochondrial mass, whereas the decrease in MMP is amplified when normalized by mitochondrial mass (Supplementary Figure 2C). Next, we found a

higher level of total ATP in relapsed allografts (Figure 2E), suggesting higher energy production during relapse.

Finally, we performed a transcriptomic study by RNA-sequencing of PDAC032T relapsed tumors compared to non-treated (controls). We applied Gene Set Enrichment Analysis (GSEA) on the RNA-seq data, and found that relapsed tumors positively correlate with changes in OXPHOS, MOOTHA_VOXPHOS, ETC and the citric acid (TCA) cycle gene signatures (Supplementary Figure 3A). Furthermore, we found that the expression of genes encoding key transcriptional regulators involved in mitochondrial homeostasis such as Peroxisome Proliferator-activated Receptor–γ Coactivator 1 alpha (*PPARGC1A*) encoding PGC-1α (but not mitochondrial transcription factor A, *TFAM*) was increased in relapsed tumors (Supplementary Figure 3B).

Collectively, these data show increases in mitochondrial and redox metabolisms in tumors that have relapsed after full treatment-induced regression compared to non-treated tumors, suggesting metabolic reprogramming imposed by the chemotherapy.

Mitochondrial metabolic reprogramming occurs during treatment-induced regression

We then asked when these changes occurred, in other words, whether they were related to tumor growth during relapse or whether they preexisted relapse. To answer this question, we analyzed xenografts during treatment before complete regression ("under treatment" setting) and at the onset of relapse ("start of relapse" setting), comparing them to untreated tumors of similar size (100-300 mm^3) (Figure 3A). We observed that all analyzed parameters were increased in both settings and in both xenografts (Figure 3B and C, and Supplementary Figure 4), as observed in relapsed tumors at the end point. Importantly, mitochondrial mass was the parameter that was most increased, explaining the attenuation or even reversal of changes in MMP and mitochondrial superoxide after normalization with mitochondrial mass (Supplementary Figure 4A and B). These data suggest that the treatment, i.e., gemcitabine alone or combined with perhexiline for PDAC032T and PDAC084T xenografts, respectively, could promote the survival of treatment-adapted cells while inducing the death of most tumor cells by oxidative stress associated with the treatment. Indeed, *in vitro*

treatments induce an increase in ROS that can be prevented by supplementation with the antioxidant NAC, and a redox-induced loss of cell viability (Supplementary Figure 5).

Overall, these data show that chemotherapy treatment affects mitochondrial and redox metabolisms, and suggest that some cells that survive through metabolic adaptations (so-called residual or persistent cells) may be responsible for the relapse.

Antioxidant defenses are increased in relapsed tumors and in tumors during treatment

A crucial metabolic adaptation observed in cancer cells during tumor development is the exacerbation of antioxidant defenses to cope with the increased production of ROS, which allows the survival of the adapted cells [29,30]. This adaptation is also observed during oxidative stress induced by chemotherapy or radiotherapy. The main antioxidant defenses are antioxidant enzymes such as glutathione peroxidases (GPX), superoxide dismutases, and catalase, as well as small antioxidant molecules such as glutathione and NADPH that are found to be abundant in cancer cells (schematic in Figure 4A). In addition, the nuclear factor erythroid 2-related factor 2 (Nrf2) plays a crucial role in antioxidant gene expression; it can be controlled both at the level of expression and cellular localization since it is translocated to the nucleus only when ROS levels increase. One of the target genes of Nrf2 is *Slc7a11*, which encodes the cystine/glutamate transporter (xCT), which allows the entry of cystine into cells as a precursor of glutathione. We first quantified glutathione and NADPH in xenografts at relapse end point, and found increased total levels as well as increased ratio reduced/oxidized glutathione (GSH/GSSG) (Figure 4B and Supplementary Figure 6). We then analyzed expression of several antioxidant genes: *Nrf2*, its target *HO-1*, *Slc7a11*, and *GPX4*. These four genes were found to be overexpressed in the relapse endpoint context (Figure 4C).

We then measured the expression of these genes by RT-qPCR in xenografts under treatment and at the onset of relapse (Figure 4D and E). *Nrf2* was not found to be overexpressed in these settings, unlike its target gene *HO-1*, suggesting that Nrf2 is activated even when not overexpressed. The *Slc7a11* and *GPX4* genes were found

overexpressed in all conditions (although some differences did not reach statistical significance).

We also examined the expression of genes encoding proteins involved in mitochondrial homeostasis (PGC-1α and TFAM) and found them overexpressed in most of the conditions analyzed (Figure 4F), suggesting that increased mitochondrial mass plays a role in mitochondrial ROS overproduction, generating oxidative stress that is counterbalanced by increased antioxidant defenses.

Collectively, these data suggest that the persister cells responsible for relapse originate from cells that have adapted to drug-induced oxidative stress by increasing antioxidant defenses.

ROS accumulation is a vulnerability amenable for targeting to prevent relapse

The property of cancer cells to have a high ROS content can be used therapeutically by further increasing the level of ROS to reach the threshold for induction of cell death [29,30]. This was the course of action we took in an attempt to further increase the level of ROS in persister cells to prevent relapse. To this end, we started treatment just after the end of chemotherapy with arsenic trioxide (ATO) known to increase ROS production by inhibiting mitochondrial OXPHOS [31]. ATO treatment was performed for 1, 2 or 3 months in PDAC032T xenograft (Figure 5A). We observed that ATO was able to delay relapse compared with control (relapse of non-ATO-treated mice) in the case of mice treated with ATO for 1 month. Tumor growth started to resume before the end of treatment in the case of mice treated with ATO for 2 months and 3 months, suggesting escape from ATO treatment. We analyzed mitochondrial characteristics and ROS level in recurrent tumors and found an increase in mitochondrial mass, MMP, and ROS level in ATO-treated recurrent tumors treated for 1 month compared with the control (Figure 5B). In contrast, these characteristics decreased in recurrent ATO-treated tumors treated for 2 or 3 months compared with the control group. Finally, mitochondrial MMP and superoxide anions levels decreased in ATO-treated recurrent tumors at all time points when normalized by mitochondrial mass (Supplementary Figure 7), as well as ATP level (Figure 5B), suggesting an ATO-induced energy crisis consistent with its role in inhibiting mitochondrial respiration.

In PDAC084T xenograft, ATO treatment was performed for 2 months (Figure 5C). We observed that ATO was able to delay relapse compared with control (relapse of ATO-untreated mice). Tumor growth started to resume before the end of treatment, suggesting escape from ATO treatment. We analyzed mitochondrial characteristics and ROS level in relapsed tumors, and found increased MMP and ROS level as well as ATP level compared with control (Figure 5D), without any change of mitochondrial mass and mitochondrial superoxide, suggesting higher energy production.

Next, we explored the possibility of greater efficacy in relapse prevention by combining ATO-induced increase in ROS with decrease in antioxidant defenses, based on previous studies suggesting that redox combination therapy is a clinically promising approach in the treatment of advanced solid tumors [32]. We chose to combine ATO with buthionine sulfoximine (BSO), an inhibitor of glutathione synthesis. BSO treatment was started slightly later than ATO treatment and was performed for 2 months in both xenografts. Importantly, we observed that the combination of ATO and BSO completely prevented relapse in both PDAC xenografts (Figure 5E and F). We did not observe any relapse during the three months following the end of the combined treatment (we sacrificed the mice at this time). These data suggest that the combination of promotion of ROS production (ATO) and inhibition of antioxidant capacity (BSO) might be a promising strategy to prevent PDAC relapse.

DISCUSSION

New therapies that effectively eradicate resistant cancer cells and residual cells after a therapeutic response are an urgent medical need. This study provides evidence that targeting adaptations in redox metabolism that occur during treatment is a promising therapeutic approach to prevent relapse in PDAC.

The basis of our work is the characterization of mitochondrial and redox characteristics in pancreatic tumors in the context of therapeutic relapse (Supplementary Figure 8). We used two different PDAC mouse models: heterotopic xenografts (immunodeficient context) and orthotopic syngeneic allografts (immunocompetent context), both of which respond to chemotherapeutic treatment but relapse after complete regression. Our results demonstrated increased mitochondrial mass and higher ATP level in relapsed tumors compared to controls in both contexts. These changes were accompanied by an accumulation of mitochondrial ROS and total ROS in relapsed tumors. Same changes were observed before the growth of relapsed tumors, i.e. during treatment and at the onset of relapse in both xenografts, suggesting that the treatment (Gemcitabine alone or in combination with Perhexiline) could induce the appearance of treatment-adapted cells while inducing cell death of most of tumor cells. Thus, persister PDAC cells display increased mitochondrial mass, active polarized mitochondria, increased ATP production, and high ROS levels. Overall, our results support our initial hypothesis of chemotherapy-induced metabolic reprogramming.

Data in the literature report that cancer cells with high ATP production show upregulation of mitochondrial proteins and other protein biomarkers and are phenotypically the most aggressive, with enhanced stem-like properties, multidrug resistance, and increased capacity for metastasis [33]. In addition, it has also been suggested that higher levels of intracellular ATP may explain acquired resistance to oxaliplatin and cisplatin in colon and ovarian cancer through a variety of mechanisms, including increased glycolysis and/or mitochondrial metabolism [34,35]. A previous published work on acute myelogenous leukemia (AML) also showed that persister chemoresistant leukemic cells exhibited a high OXPHOS gene signature, high ROS levels with modified intracellular redox status, increased mitochondrial mass, and retained active polarized mitochondria [10–14,36]. All these observations suggest the

important role of mitochondrial metabolism that supports residual disease and resistance.

Recently, the modulation of ROS, mainly produced by mitochondria, in cancer cells has received significant attention and may represent a viable strategy to overcome cancer relapse [37]. In particular, studies have shown that high anti-oxidant capacity, due to increased levels of reduced glutathione, elevated NADPH, and activated Nrf2signaling, significantly contributes to the onset of multi-drug resistance [38]. Moreover, it has been shown that Nrf2 activation promotes the recurrence of dormant tumor cells through regulation of redox and nucleotide metabolism. Thus the authors demonstrated that the activation of Nrf2 in persistent dormant cells re-established higher glutathione/oxidized glutathione (GSH/GSSG) ratio, which is a major contributing factor to drug resistance [17,39] inducing relapse [15]. Our data show an increase in GSH/GSSG ratio and NADPH levels in relapsing tumors at ethical limit point. Moreover, we demonstrate that residual cells responsible of relapse adapt during treatment-induced oxidative stress by overexpressing antioxidant genes: *Nrf2*, *HO-1*, *SLC7a11*, and *GPX4*. Thus, this molecular analysis reveals that one metabolic adaptation observed in pancreatic cancer cells during treatment is exacerbation of antioxidant defenses to cope with ROS accumulation, allowing survival of adapted cells. This findings are consistent with other studies showing the role of Nrf2 in promoting cancer chemoresistance and recurrence by reprogramming cellular metabolism in breast and ovarian cancer [40,41].

Next, we found an overexpression of genes encoding proteins involved in mitochondrial homeostasis, *PGC-1α* and *TFAM* in most of the analyzed conditions, suggesting that persistent cells adapt through an increase in mitochondrial biogenesis and mitochondrial genome. Data in the literature report PGC-1α and TFAM as putative markers of chemoresistance in epithelial ovarian carcinoma [42], breast cancer [43], and hepatocellular carcinoma [44].

To prevent relapse in PDAC, we further chose to combine Arsenic Trioxide (ATO), which induces oxidative stress alone to Buthionine Sulfoximine (BSO), inhibitor of glutathione synthesis, according to previous studies suggesting the combinatory treatment as a clinically promising approach in the treatment of advanced solid tumors [32,45,46]. We observed that ATO was able to delay the relapse in the two xenograft models, but some tumor escape from the treatment and relapse. Excitingly, we

observed that the combination of BSO with ATO completely prevents relapse. This observation was consistent with *in vivo* studies on prostate cancer using a mouse orthotopic metastasis model, showing that the combination of ATO and BSO induced tumor growth inhibition in both primary and metastatic lesions, and that this combination therapy prolonged survival rate significantly. Furthermore, BSO has been demonstrated as an effective sensitizer of ATO-induced cell death [32] and the combinatory treatment succeeded in overcoming the resistance [47].

Collectively, combining the promotion of ROS production and the inhibition of antioxidant capacity could be a promising avenue for the treatment of pancreatic cancer in the clinic.

FIGURE LEGENDS

Figure 1. Mitochondrial and redox metabolisms are reprogrammed in relapsed PDAC xenografts. (A) Schematic of experimental protocol. Pieces of tumor from PDX were implanted in the subcutaneous space of recipient female Swiss nude mice. When tumors reached 200 mm^3 volume, mice were assigned to treatment groups and treated for one month. After one month, the treatment was stopped and the recurrence was followed. Mice were sacrificed according to the ethical limit point. **(B)** Tumor volume in two different PDAC xenografts (PDAC084T and PDAC032T) treated during one month with Gemcitabine (120 mg/kg IP twice a week), Gemcitabine plus Perhexiline (120 mg/kg IP twice a week and 5 mg/kg IP every other day, respectively), and Control. PDAC xenografts always relapse after complete regression induced by the chemotherapy, Gemcitabine alone or combined with Perhexiline for PDAC032T (right) and PDAC084T (left), respectively. **(C)** Mitochondrial mass (Mito mass), mitochondrial membrane potential (MMP), mitochondrial superoxide anions (Mito O2.-) and total reactive oxygen species (Total ROS) levels were measured by flow cytometry with the MitoTracker DeepRed, TMRM, MitoSOX red, and CellROX orange fluorescent probes, respectively, in relapsed tumors at ethical limit point. Median fluorescence intensity (MFI) is shown relative to that of unlabeled cells. **(D)** Total ATP level and percentages of mitochondrial and glycolytic ATP were measured using the Cell viability assay (Cell-Titer Glo Kit). For this, specific inhibitors were used: oligomycin (1µM) and 2-DG (100mM) to determine percentages of mitochondrial and glycolytic ATP, respectively. The unpaired student's T- test was used for statistical analyzes comparing each group with the untreated group. *, **, *** and **** correspond to $p<0.05$, 0.01, 0.001, and 0.0001, respectively; ns: non-significant difference.

Figure 2. Mitochondrial and redox metabolism are reprogrammed in relapsed PDAC allografts. (A) Schematic of experimental protocol. Orthotopic syngeneic allografts were generated by intraperitoneal injection of one million of the murine cells KPC luc2 into 6-week-old female C57BL/6 immunocompetent mice. Tumoral growth was followed by bioluminescence using a Photon Imager device (Biospace Lab). Twelve days post-grafting, tumor-bearing mice were randomized to two treatments cohorts (at least n = 5 per condition), vehicle control (treated with PBS) and

Gemcitabine 120 mg/kg twice a week by intraperitoneal injection during one month. Mice were sacrificed according to the ethical limit point**. (B-C)** Representative *in vivo* bioluminescence imaging data (**B**) and bioluminescent signal quantification (**C**), at different times after orthotopic implantation of KPCluc2 cells untreated (Control) or treated with Gemcitabine. The tumors of mice 1, 2, 3, 4, 5, 7 and 8 regressed during treatment with Gem but not completely (Gem group); their number is in pink color. However, those of mice 6, 9, 10, 11, and 12 regressed completely (Gem-CR group); their number is in purple. The bioluminescent signal is expressed in photons per second per square centimeter per steradian (ph/s/cm^2/sr). **(D)** Mitochondrial mass, MMP, Mitochondrial O2.- and total ROS level were measured in tumors as in Figure 1. Median fluorescence intensity (MFI) is shown relative to unlabeled cells. **(E)** Total ATP level was measured using the cell viability assay (Cell-Titer Glo Kit). The unpaired student's T- test was used for statistical analyzes comparing each group with that of the untreated. *, **, *** and **** correspond to $p<0.05$, 0.01, 0.001, and 0.0001, respectively; ns: non-significant difference.

Figure 3. Mitochondrial metabolic reprogramming occurs during treatment-induced regression in PDAC xenografts. (A) Tumor volume in PDAC084T (top), and PDAC032T (bottom) during Gem+Perx or Gem treatment alone, respectively, before complete regression ("under treatment" context) and at the onset of relapse ("start of relapse" context), compared to non-treated tumors (Control) of similar size (100-300 mm^3). For the control groups, we show the measurement of tumor volumes from two weeks after inoculation. For the treated groups, we show the measurement of tumor volumes from the start of treatment. **(B-C)** Mitochondrial mass, MMP, Mitochondrial O2.- and total ROS level were measured in tumors under treatment **(B)** and at the start of relapse **(C).** Total and mitochondrial ATP were measured in both context **(B-C)** using cell viability assay (Cell-Titer Glo Kit). Significance was determined by Student's T-test. *, **, *** and **** correspond to $p<0.05$, 0.01, 0.001, and 0.0001, respectively; ns: non-significant difference.

Figure 4. Antioxidant defenses are increased in relapsed tumors and in tumors during treatment.

(A) Simplified schematic representation of ROS generation and enzymatic antioxidant defenses. Superoxide anion ($O_2^{\cdot -}$) is mainly produced by the mitochondrial ETC complexes by partial reduction of molecular oxygen (O_2). Superoxide is dismutated into hydrogen peroxide (H_2O_2) by superoxide dismutases (SOD). H_2O_2 is converted to water (H_2O) by glutathione peroxidases (GPX). Via the Fenton reaction with metal ions Fe^{2+} or Cu^{+}, H_2O_2 is further reduced to highly reactive hydroxyl radical ($OH^{\cdot}$), thereby damaging biological macromolecules such as DNA, lipids, and proteins. H_2O_2 is the main player in redox homeostasis, and can induce the activation of the antioxidant transcription factor Nrf2 through dissociation of the Nrf2-KEAP1 complex, phosphorylation of Nrf2, and its nuclear translocation. In the nucleus, Nrf2 promotes transcription of multiple antioxidant genes such as *SLC7A11* and *HO-1* by binding to the antioxidant responsive elements (ARE) in the promoter region of target genes. Via its entry into cells through the glutamate/cystine antiporter xCT encoded by the *SLC7A11* gene, cysteine can enhance GSH production which is a tripeptide glutamate-cysteine-glycine. The antioxidant function of GSH is mediated by two enzymes: GPX and GR. GPX allows the reduction of H_2O_2 by the oxidation of GSH (reduced glutathione) to GSSG (oxidized glutathione). The GSSG is subsequently reduced to GSH by GR at the expense of NADPH used as a cofactor. **(B)** Ratio of reduced glutathione (GSH) / oxidized glutathione (GSSG), and NADPH levels were measured in PDAC relapsed tumor. **(C-D-E)** RT-qPCR analysis of antioxidant gene expression: *Nrf2*, *HO-1*, *SLC7A11* and *GPX4*, in relapsed PDAC tumors at endpoint (**C**), under treatment (**D**) and start of relapse (**E**). **(F)** The mRNA levels of PGC-1α and TFAM was monitored by RT-qPCR in relapsed PDAC tumors under treatment and start of relapse, respectively. Data are representative of 3 independent qPCR experiments. Significance was determined by Student's T-test. *, **, *** and **** correspond to $p<0.05$, 0.01, 0.001, and 0.0001, respectively; ns: non-significant difference.

Figure 5. Targeting redox metabolism prevents relapse in both PDAC xenografts. **(A)** Tumor volume in PDAC032T xenograft treated with ATO (5 mg/kg/day) for one, two or three months starting just after the end of chemotherapy-induced complete regression. **(B)** Mitochondrial mass, MMP, Mitochondrial O2.- and total ROS level were measured in PDAC032T xenografts (Top). Median fluorescence intensity (MFI) is shown relative to unlabeled cells. Total ATP level, percentage of mitochondrial and

glycolytic ATP were measured using the Cell viability assay (Cell-Titer Glo Kit) in PDAC032T (Bottom). Specific inhibitors were used: oligomycin (1µM) and 2-DG (100mM) to determine mitochondrial and glycolytic ATP, respectively. **(C)** Tumor volume in PDAC084T xenograft treated with ATO (5 mg/kg/day) for two months starting after the end of combinatory therapy-induced complete regression. **(D)** Mitochondrial mass, MMP, Mitochondrial O2.- and total ROS level were measured in PDAC084T xenografts. Total ATP level was measured using the Cell viability assay (Cell-Titer Glo Kit). **(E and F)** Tumor volume in PDAC032T (**E**) and PDAC084T (**F**) xenografts, respectively, treated with ATO (5 mg/kg/day) and BSO (30 mg/kg) during two months starting after the end of chemotherapy-induced complete regression. The Unpaired T-test was used for statistical analyzes comparing each group with the untreated group. *, ** and *** $p<0.05$, 0.01, 0.001, respectively; ns: non-significant difference.

REFERENCES

1. Rahib, L. *et al.* Projecting Cancer Incidence and Deaths to 2030: The Unexpected Burden of Thyroid, Liver, and Pancreas Cancers in the United States. *Cancer Res.* **74**, 2913 (2014).
2. Saad, A. M., Turk, T., Al-Husseini, M. J. & Abdel-Rahman, O. Trends in pancreatic adenocarcinoma incidence and mortality in the United States in the last four decades; a SEER-based study. *BMC Cancer* **18**, 688 (2018).
3. Siegel, R. L., Miller, K. D. & Jemal, A. Cancer statistics, 2020. *CA. Cancer J. Clin.* **70**, 7–30 (2020).
4. Roser, M. & Ritchie, H. Cancer. *Our World Data* (2015).
5. Conroy, T. *et al.* FOLFIRINOX or Gemcitabine as Adjuvant Therapy for Pancreatic Cancer. *N. Engl. J. Med.* **379**, 2395–2406 (2018).
6. Nevala-Plagemann, C., Hidalgo, M. & Garrido-Laguna, I. From state-of-the-art treatments to novel therapies for advanced-stage pancreatic cancer. *Nat. Rev. Clin. Oncol.* **17**, 108–123 (2020).
7. Wang, X., Zhang, H. & Chen, X. Drug resistance and combating drug resistance in cancer. *Cancer Drug Resist.* **2**, 141–160 (2019).
8. Pan, S.-T., Li, Z.-L., He, Z.-X., Qiu, J.-X. & Zhou, S.-F. Molecular mechanisms for tumour resistance to chemotherapy. *Clin. Exp. Pharmacol. Physiol.* **43**, 723–737 (2016).
9. Shen, S., Vagner, S. & Robert, C. Persistent Cancer Cells: The Deadly Survivors. *Cell* **183**, 860–874 (2020).
10. Bosc, C. *et al.* Mitochondrial inhibitors circumvent adaptive resistance to venetoclax and cytarabine combination therapy in acute myeloid leukemia. *Nat. Cancer* **2**, 1204–1223 (2021).
11. Goldman, A. *et al.* Targeting tumor phenotypic plasticity and metabolic remodeling in adaptive cross-drug tolerance. *Sci. Signal.* **12**, eaas8779 (2019).

12. Kuntz, E. M. *et al.* Targeting mitochondrial oxidative phosphorylation eradicates therapy-resistant chronic myeloid leukemia stem cells. *Nat. Med.* **23**, 1234–1240 (2017).

13. Roesch, A. *et al.* Overcoming intrinsic multi-drug resistance in melanoma by blocking the mitochondrial respiratory chain of slow-cycling JARID1Bhigh cells. *Cancer Cell* **23**, 10.1016/j.ccr.2013.05.003 (2013).

14. Zaretsky, J. M. *et al.* Mutations Associated with Acquired Resistance to PD-1 Blockade in Melanoma. *N. Engl. J. Med.* **375**, 819–829 (2016).

15. Fox, D. B. *et al.* NRF2 activation promotes the recurrence of dormant tumour cells through regulation of redox and nucleotide metabolism. *Nat. Metab.* **2**, 318–334 (2020).

16. Hangauer, M. J. *et al.* Drug-tolerant persister cancer cells are vulnerable to GPX4 inhibition. *Nature* **551**, 247–250 (2017).

17. Traverso, N. *et al.* Role of glutathione in cancer progression and chemoresistance. *Oxid. Med. Cell. Longev.* **2013**, 972913 (2013).

18. Viswanathan, V. S. *et al.* Dependency of a therapy-resistant state of cancer cells on a lipid peroxidase pathway. *Nature* **547**, 453–457 (2017).

19. Zhang, X. *et al.* Glutathione Peroxidase 4 as a Therapeutic Target for Anti-Colorectal Cancer Drug-Tolerant Persister Cells. *Front. Oncol.* **12**, 913669 (2022).

20. Alistar, A. *et al.* Safety and tolerability of the first-in-class agent CPI-613 in combination with modified FOLFIRINOX in patients with metastatic pancreatic cancer: a single-centre, open-label, dose-escalation, phase 1 trial. *Lancet Oncol.* **18**, 770–778 (2017).

21. Daemen, A. *et al.* Metabolite profiling stratifies pancreatic ductal adenocarcinomas into subtypes with distinct sensitivities to metabolic inhibitors. *Proc. Natl. Acad. Sci.* **112**, E4410–E4417 (2015).

22. Hollinshead, K. E. R. *et al.* Respiratory Supercomplexes Promote Mitochondrial Efficiency and Growth in Severely Hypoxic Pancreatic Cancer. *Cell Rep.* **33**, 108231 (2020).

23. Masoud, R. *et al.* Targeting Mitochondrial Complex I Overcomes Chemoresistance in High OXPHOS Pancreatic Cancer. *Cell Rep. Med.* **1**, 100143 (2020).

24. Sancho, P. *et al.* MYC/PGC-1α Balance Determines the Metabolic Phenotype and Plasticity of Pancreatic Cancer Stem Cells. *Cell Metab.* **22**, 590–605 (2015).

25. Cohen, R. *et al.* Targeting cancer cell metabolism in pancreatic adenocarcinoma. *Oncotarget* **6**, 16832–16847 (2015).

26. Reyes-Castellanos, G., Masoud, R. & Carrier, A. Mitochondrial Metabolism in PDAC: From Better Knowledge to New Targeting Strategies. *Biomedicines* **8**, 270 (2020).

27. Viale, A. *et al.* Oncogene ablation-resistant pancreatic cancer cells depend on mitochondrial function. *Nature* **514**, 628–632 (2014).

28. Viale, A., Corti, D. & Draetta, G. F. Tumors and Mitochondrial Respiration: A Neglected Connection. *Cancer Res.* **75**, 3687–3691 (2015).

29. Cairns, R. A., Harris, I. S. & Mak, T. W. Regulation of cancer cell metabolism. *Nat. Rev. Cancer* **11**, 85–95 (2011).

30. Gorrini, C., Harris, I. S. & Mak, T. W. Modulation of oxidative stress as an anticancer strategy. *Nat. Rev. Drug Discov.* **12**, 931–947 (2013).

31. Diepart, C. *et al.* Arsenic trioxide treatment decreases the oxygen consumption rate of tumor cells and radiosensitizes solid tumors. *Cancer Res.* **72**, 482–490 (2012).

32. Maeda, H. *et al.* Effective treatment of advanced solid tumors by the combination of arsenic trioxide and L-buthionine-sulfoximine. *Cell Death Differ.* **11**, 737–746 (2004).

33. Fiorillo, M., Ózsvári, B., Sotgia, F. & Lisanti, M. P. High ATP Production Fuels Cancer Drug Resistance and Metastasis: Implications for Mitochondrial ATP Depletion Therapy. *Front. Oncol.* **11**, 740720 (2021).

34. Zhou, Y. *et al.* Intracellular ATP levels are a pivotal determinant of chemoresistance in colon cancer cells. *Cancer Res.* **72**, 304–314 (2012).

35. Schneider, V., Krieger, M. L., Bendas, G., Jaehde, U. & Kalayda, G. V. Contribution of intracellular ATP to cisplatin resistance of tumor cells. *J. Biol. Inorg. Chem. JBIC Publ. Soc. Biol. Inorg. Chem.* **18**, 165–174 (2013).

36. Farge, T. *et al.* Chemotherapy-Resistant Human Acute Myeloid Leukemia Cells Are Not Enriched for Leukemic Stem Cells but Require Oxidative Metabolism. *Cancer Discov.* **7**, 716–735 (2017).

37. Cui, Q. *et al.* Modulating ROS to overcome multidrug resistance in cancer. *Drug Resist. Updat. Rev. Comment. Antimicrob. Anticancer Chemother.* **41**, 1–25 (2018).

38. Cort, A., Ozben, T., Saso, L., De Luca, C. & Korkina, L. Redox Control of Multidrug Resistance and Its Possible Modulation by Antioxidants. *Oxid. Med. Cell. Longev.* **2016**, 4251912 (2016).

39. Zhu, Z. *et al.* Glutathione reductase mediates drug resistance in glioblastoma cells by regulating redox homeostasis. *J. Neurochem.* **144**, 93–104 (2018).

40. Deng, X. *et al.* The Nrf2/PGC1α Pathway Regulates Antioxidant and Proteasomal Activity to Alter Cisplatin Sensitivity in Ovarian Cancer. *Oxid. Med. Cell. Longev.* **2020**, 4830418 (2020).

41. Syu, J.-P., Chi, J.-T. & Kung, H.-N. Nrf2 is the key to chemotherapy resistance in MCF7 breast cancer cells under hypoxia. *Oncotarget* **7**, 14659–14672 (2016).

42. Gabrielson, M., Björklund, M., Carlson, J. & Shoshan, M. Expression of mitochondrial regulators PGC1α and TFAM as putative markers of subtype and chemoresistance in epithelial ovarian carcinoma. *PloS One* **9**, e107109 (2014).

43. Andrzejewski, S. *et al.* PGC-1α Promotes Breast Cancer Metastasis and Confers Bioenergetic Flexibility against Metabolic Drugs. *Cell Metab.* **26**, 778-787.e5 (2017).

44. Zhu, Y. *et al.* TFAM depletion overcomes hepatocellular carcinoma resistance to doxorubicin and sorafenib through AMPK activation and mitochondrial dysfunction. *Gene* **753**, 144807 (2020).

45. Ong, P.-S., Chan, S.-Y. & Ho, P. C. Differential augmentative effects of buthionine sulfoximine and ascorbic acid in As2O3-induced ovarian cancer cell death: oxidative stress-independent and -dependent cytotoxic potentiation. *Int. J. Oncol.* **38**, 1731–1739 (2011).

46. Wang, T. *et al.* [Arsenic trioxide combined with buthionine sulfoximine enhances apoptosis in multidrug-resistant human leukemia K562/ADM cells in vitro]. *Zhonghua Zhong Liu Za Zhi* **30**, 188–191 (2008).

47. Akhtar, A., Wang, S. X., Ghali, L., Bell, C. & Wen, X. Recent advances in arsenic trioxide encapsulated nanoparticles as drug delivery agents to solid cancers. *J. Biomed. Res.* **31**, 177–188 (2017).

SUPPLEMENTARY MATERIAL

Supplementary Methods and Materials

Transcriptomic analysis by bulk RNA sequencing

Total RNA Isolation from tumors

Total RNA was isolated from 20-25 mg of tumor piece using both TRIzol (Invitrogen) and the Qiagen total RNA isolation kit (Qiagen, ref 74004) to avoid protein and extracellular matrix accumulation in the columns. Briefly, tumor piece was lysed in 600 µL RLT Buffer (from Qiagen kit) with 1% β-Mercaptoethanol using beads tube from Precellys lysing kit for hard tissue (ref P000917-LYSK0-A, 3x Cycle 1500 rpm, 15 sec of mix, 10 sec of rest) and directly centrifuged 3 min at 10.000g at RT. Supernatant was transferred in 400µL of TRIzol and incubated for 5 min at RT followed by addition of 150µL of Chloroforme. Tubes were carefully mixed and incubated 3 min at RT before centrifugation (12.000g, 5min, 4°C). The transparent upper phase containing RNAs was transferred in a tube containing 500 µL of 70% Ethanol, mixed and transferred inside Qiagen RNA isolation kit columns according to manufacturer's instructions followed until the end of extraction. RNA integrity and concentration were assessed using the Agilent 2100 Bioanalyzer (Agilent Technologies, Palo Alto, CA). The average RIN (RNA integrity number) values for all samples was comprised between 9.3 and 10, ensuring a high quality of isolated RNAs.

Bulk RNA sequencing

The preparation of mRNA libraries was realized following manufacturer's recommendations (kapa mRNA HyperPrep from ROCHE). Final samples pooled library prep were sequenced on ILLUMINA Novaseq 6000 with S1-200cycles cartridge (2x1600Millions of 100 bases reads), corresponding to 2x30Millions of reads per sample after demultiplexing.

Bulk RNA sequencing data analysis

Quality control has been performed on the fastq files using FastQC (v0.11.9) (http://www.bioinformatics.babraham.ac.uk/projects/fastqc). To map the sequenced

reads to the human reference genome, we made use of STAR (v2.7.3a). From these mapped reads, gene counts were then quantified using featureCounts (v2.0.1). Starting from the raw gene counts, normalization and differential expression analysis have then been performed using DESeq2 (v 1.22.2).

Gene Set Enrichment Analysis (GSEA)

Gene set enrichment analysis (GSEA) was performed using GSEA v4.1 tool (Broad Institute). Following parameters were used: Number of permutations = 1000, permutation type = gene set, Chip = Human_Ensembl_Gene_ID_MSigDB.v2022.1.Hs.chip. Other parameters were left at default values. The normalized enrichment scores (NES) were computed from PDAC032T relapse group compared to PDAC032T control group. Genes with FDR q-value < 0.05 and fold change >= 1.5 were considered of interest.

Supplementary Figures

Supplementary Figure 1. Representative flow cytometry plots of tumor cells populations from xenograft and allograft mouse models (related to Figures 1 and 2). Tumor cells are separated from debris by Forward Scatter Area (FSC-A)/Side Scatter Area (SSC-A), and doublets are excluded by FSC-A and FSC-height (FSC-H) dot plots. In xenograft model, Mitotracker deep Red, CellRox Orange, MitoSOX Red, and TMRM histograms are done by gating on single cells **(A).** In allograft model, the histograms are done by gating on GFP^+ cells (KPCluc2 cancer cells) after gating on live cells (the negative fractions for VioBlue-A staining) **(B).**

Supplementary Figure 2. Mitochondrial and redox metabolic reprogramming imposed by chemotherapy in relapsed PDAC xenografts (related to Figures 1 and 2). TMRM (measuring mitochondrial membrane potential) and MitoSOX (measuring mitochondrial superoxide anions) values were normalized by Mitotracker (measuring mitochondrial mass) values in relapsed xenografts (**A**), and relapsed allografts (**C**). **(B)** ATP production was measured in the presence of oligomycin (left) and 2DG (right) *in vitro* on dissociated relapsed xenografts, allowing to calculate mitochondrial and glycolytic ATP percentages shown in Figure 1D.

Supplementary Figure 3. Gene set enrichment analysis (GSEA) on RNA-seq data from PDAC032T xenografts *ex vivo*. (A) Four mitochondrial signatures were assessed by GSEA: Oxidative phosphorylation, MOOTHA_VOXPHOS, ETC, and Reactome TCA cycle and respiratory electron transport. Significant enrichments are observed in PDAC032T relapsed tumors versus control. The top portion of each panel shows the normalized enrichment scores (NES) for each signature; the bottom portion of the plot indicates the value of the ranking metric moving down the list of ranked genes. **(B)** *PPARGC1A* and *TFAM* expression in PDAC032T relapsed tumors versus control based on RNA sequencing. *$P < 0.05$; **$P < 0.01$; ***$P < 0.001$. ns, not significant.

Supplementary Figure 4. Mitochondrial and redox metabolic reprogramming occurs during treatment-induced complete regression in PDAC xenografts (related to Figure 3) (A-B) TMRM and MitoSOX values were normalized by Mitotracker values in xenografts PDAC084T (left) and PDAC032T (right), under treatment (UT, **A**) and at start of relapse (SR, **B**). **(C-D)** ATP production was measured in the presence of oligomycin and 2DG *in vitro* on dissociated relapsed xenografts PDAC084T (left) and PDAC032T (right), under treatment (UT, **C**) and at start of relapse (SR, **D**). **(E)** Percentages of glycolytic ATP in PDAC084T (left) and PDAC032T (right), under treatment (UT) and at start of relapse (SR).

Supplementary Figure 5. Chemotherapy induces ROS increases and redox-driven loss of cell viability in PDAC cells *in vitro* (related to Figure 3). (A) Total ROS level was measured by flow cytometry with the CellROX orange probe in PDAC084T and PDAC032T cells cultured *in vitro*, after 24 hours treatment with Gemcitabine (1 µM), or Perhexiline (7 µM), or combination at same concentrations. We used DMSO (0.05%) as vehicle for the controls. NAC (2.5 mM) was used as an antioxidant agent to prevent ROS accumulation; supplementation was performed for 24 hours at the same time as the treatments. Data are expressed as mean ± SEM and are representative of three independent experiments performed in duplicates. To calculate p values, Unpaired T-test was used. **(B)** Percentage of live cells treated for 24 hours with Gemcitabine (1 µM), Perhexiline (7 µM) or the combination in PDAC084T, and with Gemcitabine alone in PDAC032T. Cell viability was determined by Crystal violet assay. Data are means of triplicates ± SEM, and are representative of three independent experiments. Unpaired T-test was used. *, **, *** and **** correspond to $p<0.05$, 0.01, 0.001, and 0.0001, respectively; ns: non-significant difference.

Supplementary Figure 6. Abundance of antioxidant small molecules in xenografts at relapse end point (related to Figure 4) (A) Intracellular levels of GSH, GSSG and total GSH+GSSG levels were measured with the GSH/GSSG-Glo™ Assay| (Promega Kit). **(B)** $NADP^+$ levels, total $NADP^+$ + NADPH levels, and NADPH/$NADP^+$ ratio was measured using the NADP/NADPH-Glo™ Assay kit.

Supplementary Figure 7. Mitochondrial metabolic reprogramming during ATO treatment in PDAC xenografts (related to Figure 5) (A-B) TMRM and MitoSOX values were normalized by Mitotracker values in xenografts PDAC032T (**A, left**) and PDAC084T (**B**), and ATP production was measured in the presence of oligomycin and 2DG in vitro on dissociated xenografts PDAC032T (**A, Right**).

Supplementary Figure 8. Working model of treatment-induced acquired resistance in PDAC. In tumors that respond to therapy, most tumor cells die (dead cells) during treatment, ensuring therapy-induced regression. However, some cells survive (persistent or residual cells) during regression, through the establishment of metabolic (mitochondrial and redox) adaptations. They are maintained in the tumor scar and are associated with what is known as minimal residual disease. When these persistent (also called persister) cells resume their proliferation, they are at the origin of the regrowth and the relapse of the tumor.

Footnotes

Data availability statement All data used for this study are available from the lead contact alice.carrier@inserm.fr upon request.

Materials Availability This study did not generate new unique reagents.

Acknowledgments We thank Nathalie Auphan-Anezin (CIML) for the KPC luc2 cells, the cell culture platform (PCC, TPR2, Marseille, France) for technical assistance, and Karim Sari and Régis Vitestelle for assistance with the use of the PSEA animal housing facility. In addition, we thank Odile and Julie for their advice in cell culture, Martin Bigonnet and Yifan Jiang for their advice on the orthotopic xenografts experiments, Patricia Santofimia-Castaño for antioxidant and mitochondrial gene primers, and Fabio Marchiano for RNA-seq raw data normalization.

Contributors Conceptualization and Methodology, NAH, GR-C, and AC; Investigation, NAH, GR-C, RM, and TG; Formal Analysis, NAH, GR-C, TG, EB, JES, and AC; Resources, JI; Writing – Original Draft, NAH, and AC; Writing – Review & Editing, NAH, GR-C, RM, JI, and AC; Visualization, NAH, GR-C, RM, and AC; Supervision, AC; Project Administration and Funding Acquisition, AC.

FUNDING This work was supported by Institut National de la Santé et de la Recherche Médicale, Centre National de la Recherche Scientifique, Institut National du Cancer (INCa), Fondation ARC pour la Recherche sur le Cancer (PJA20181208207), DGOS (labellisation SIRIC), Fondation Amidex, and Fondation de France. This work also benefited from grants from Cancéropôle Provence Alpes Côte d'Azur (PACA) and Fédération GEFLUC. GR-C was supported by the CONACYT (Mexico, grant 339091 / 471717) and La Ligue Nationale contre le Cancer (LNCC), RM by the Fondation ARC pour la Recherche sur le Cancer, JG and SL by the Fondation pour la Recherche Médicale, NAH by Association AZM et Saade (Lebanon) and the Fondation pour la Recherche Médicale, TG by the French Agence Nationale pour la Recherche.

COMPETING INTERESTS The authors declare no conflicts of interests.

Figure 1

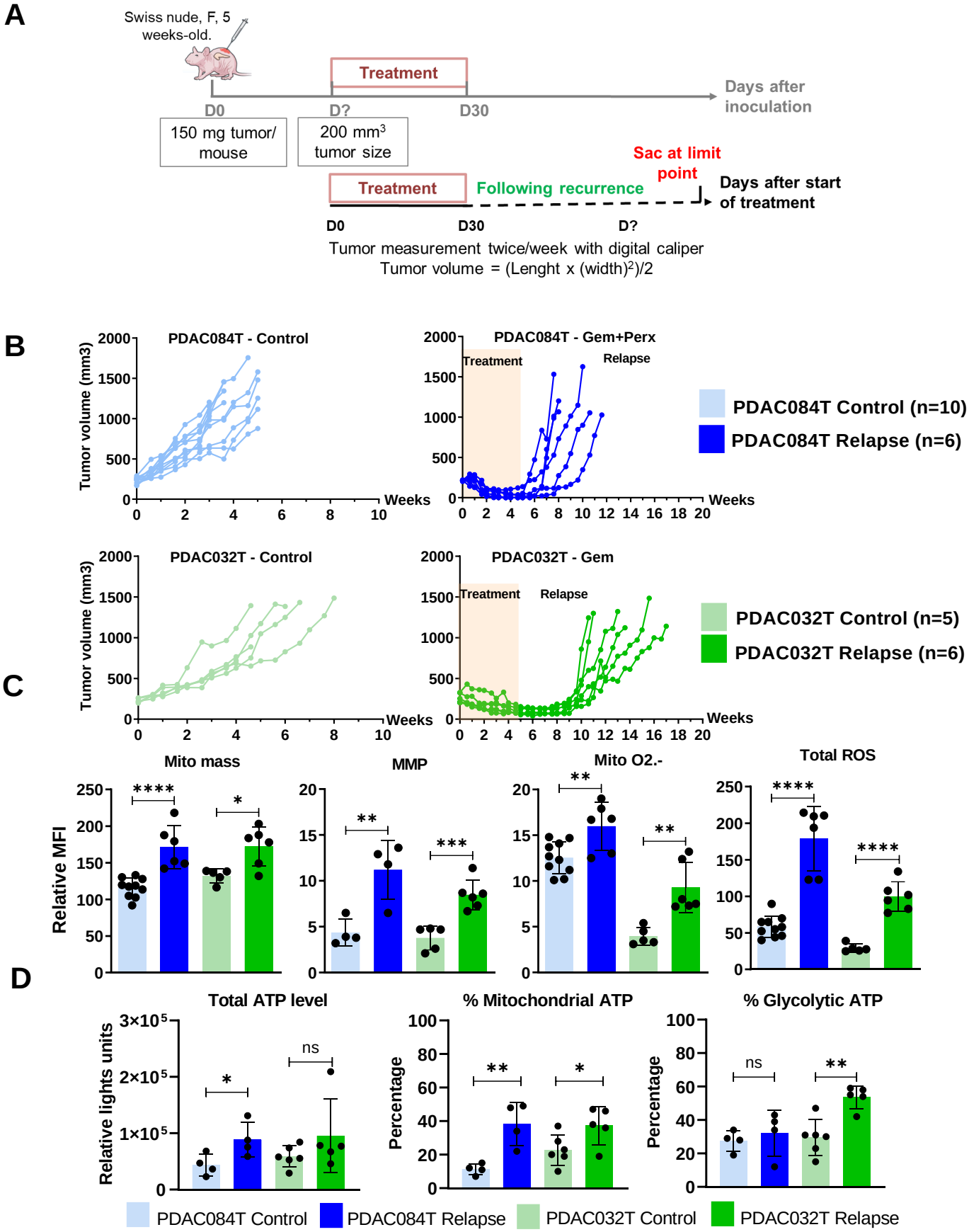
A
Swiss nude, F, 5 weeks-old.
Treatment
Days after inoculation
D0
D?
D30
150 mg tumor/ mouse
200 mm3 tumor size
Sac at limit point
Treatment
Following recurrence
Days after start of treatment
D0
D30
D?
Tumor measurement twice/week with digital caliper
Tumor volume = (Lenght x (width)2)/2
B
PDAC084T - Control
PDAC084T - Gem+Perx
Treatment
Relapse
Tumor volume (mm3)
Weeks
PDAC084T Control (n=10)
PDAC084T Relapse (n=6)
C
PDAC032T - Control
PDAC032T - Gem
Treatment
Relapse
Tumor volume (mm3)
Weeks
PDAC032T Control (n=5)
PDAC032T Relapse (n=6)
D
Mito mass
MMP
Mito O2.-
Total ROS
Relative MFI
Total ATP level
% Mitochondrial ATP
% Glycolytic ATP
Relative lights units
Percentage
ns
PDAC084T Control
PDAC084T Relapse
PDAC032T Control
PDAC032T Relapse

Figure 2

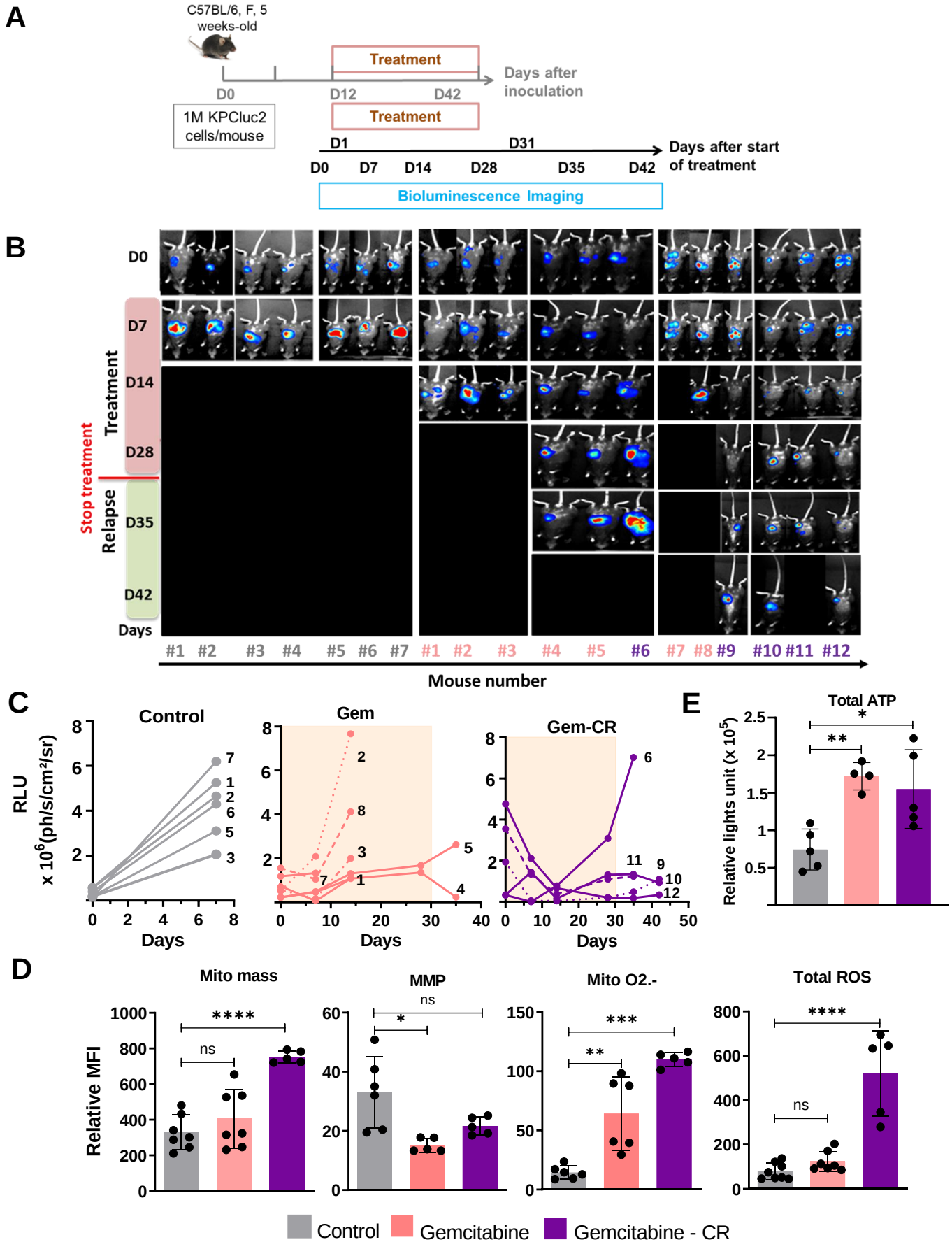
A
C57BL/6, F, 5 weeks-old
Treatment
Days after inoculation
D0
D12
D42
1M KPCluc2 cells/mouse
Treatment
D1
D31
D0 D7 D14 D28 D35 D42
Days after start of treatment
Bioluminescence Imaging
B
D0
D7
D14
D28
D35
D42
Days
Treatment
Relapse
Stop treatment
#1 #2 #3 #4 #5 #6 #7 #1 #2 #3 #4 #5 #6 #7 #8 #9 #10 #11 #12
Mouse number
C
Control
Gem
Gem-CR
RLU x 10^6(ph/s/cm²/sr)
Days
E
Total ATP
Relative lights unit (x 10^5)
D
Mito mass
MMP
Mito O2.-
Total ROS
Relative MFI
ns
Control
Gemcitabine
Gemcitabine - CR

Figure 3

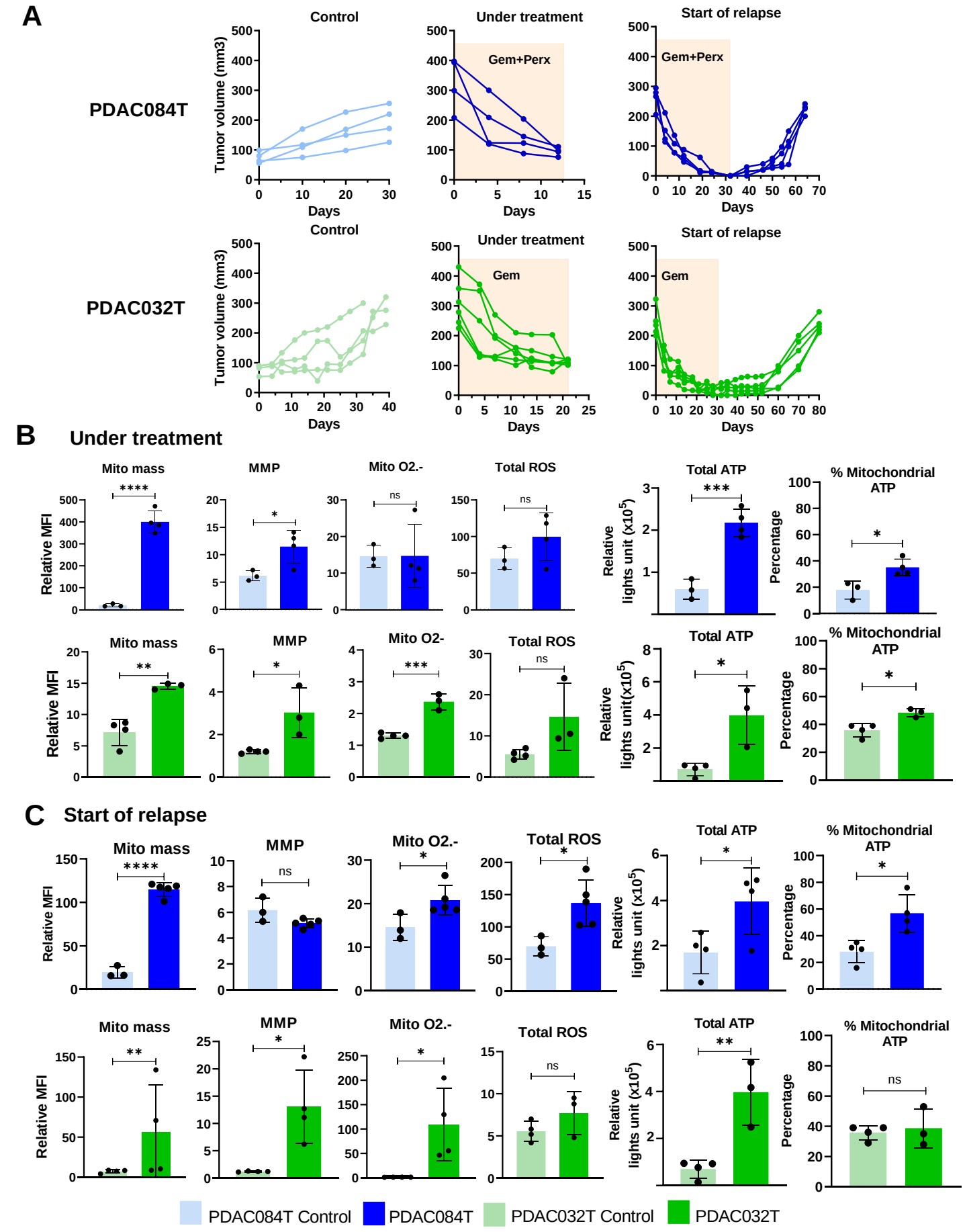
A
PDAC084T
PDAC032T
Control
Under treatment
Start of relapse
Tumor volume (mm3)
Days
Gem+Perx
Gem
B
Under treatment
C
Start of relapse
Mito mass
MMP
Mito O2.-
Total ROS
Total ATP
% Mitochondrial ATP
Relative MFI
Relative lights unit (x10^5)
Percentage
ns
PDAC084T Control
PDAC084T
PDAC032T Control
PDAC032T

Figure 4

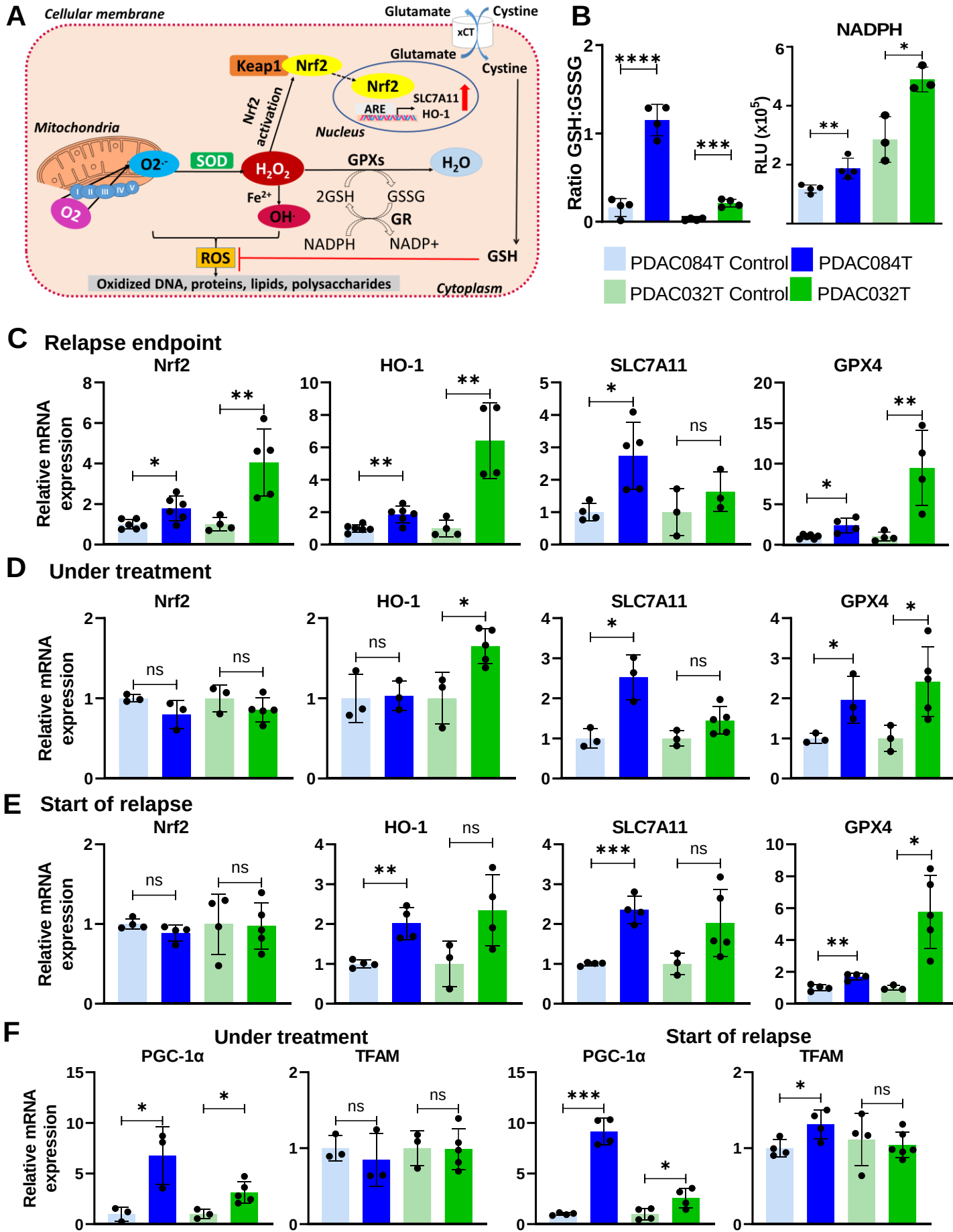
A
Cellular membrane
Glutamate
Cystine
xCT
Glutamate
Cystine
Keap1
Nrf2
Nrf2
SLC7A11
ARE
HO-1
Nrf2 activation
Nucleus
Mitochondria
O2·-
SOD
H2O2
GPXs
H2O
Fe2+
2GSH
GSSG
GR
OH·
O2
NADPH
NADP+
ROS
GSH
Oxidized DNA, proteins, lipids, polysaccharides
Cytoplasm
B
NADPH
Ratio GSH:GSSG
RLU (x10^5)
PDAC084T Control
PDAC084T
PDAC032T Control
PDAC032T
C
Relapse endpoint
Nrf2
HO-1
SLC7A11
GPX4
Relative mRNA expression
D
Under treatment
Nrf2
HO-1
SLC7A11
GPX4
Relative mRNA expression
E
Start of relapse
Nrf2
HO-1
SLC7A11
GPX4
Relative mRNA expression
F
Under treatment
Start of relapse
PGC-1α
TFAM
PGC-1α
TFAM
Relative mRNA expression

Figure 5

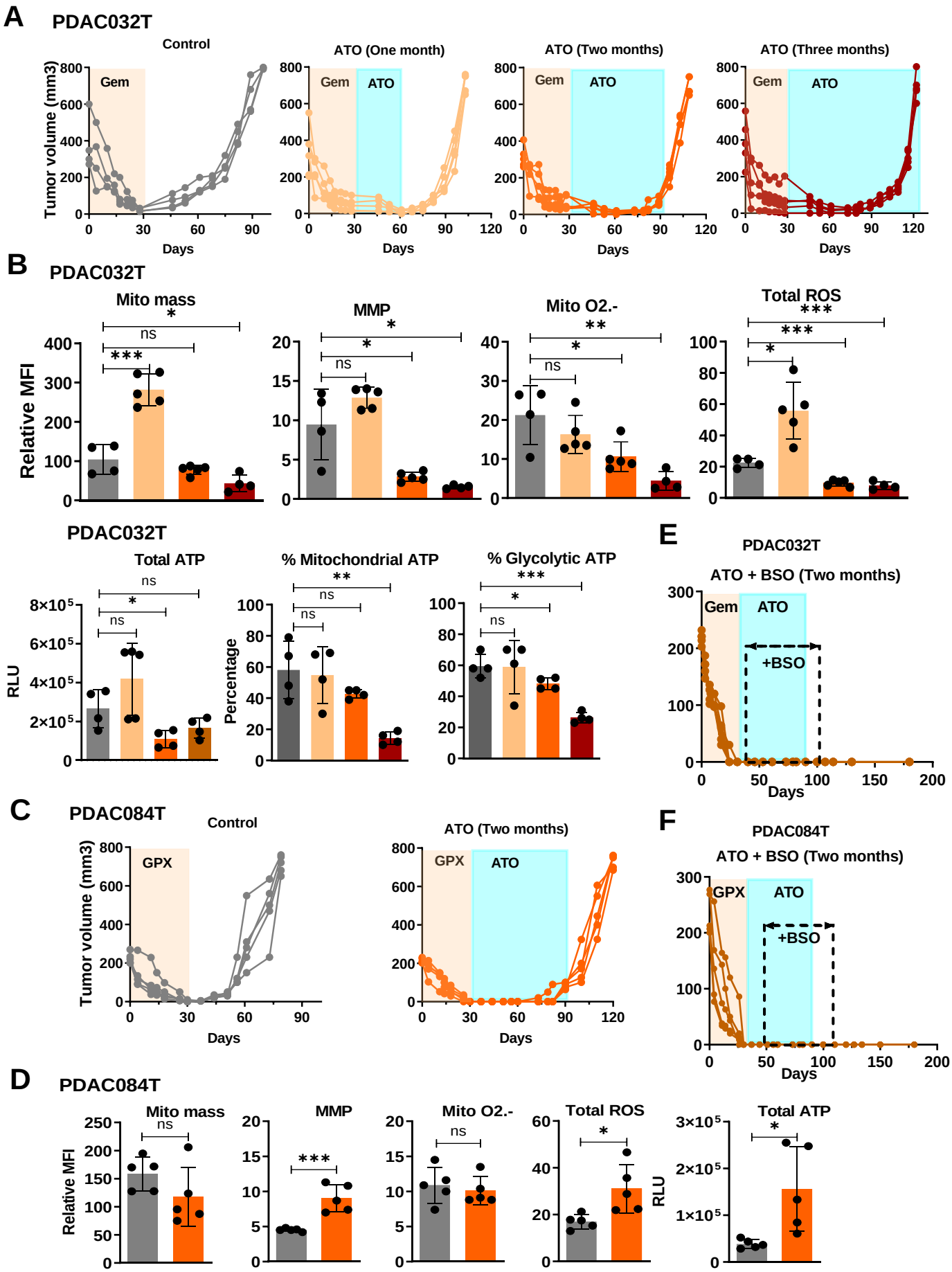
A
PDAC032T
Control
ATO (One month)
ATO (Two months)
ATO (Three months)
Gem
ATO
Tumor volume (mm3)
Days
B
PDAC032T
Mito mass
MMP
Mito O2.-
Total ROS
Relative MFI
ns
*
**
***
PDAC032T
Total ATP
% Mitochondrial ATP
% Glycolytic ATP
RLU
Percentage
E
PDAC032T
ATO + BSO (Two months)
+BSO
C
PDAC084T
Control
ATO (Two months)
GPX
F
PDAC084T
ATO + BSO (Two months)
D
PDAC084T
Mito mass
MMP
Mito O2.-
Total ROS
Total ATP

Supplementary Figure 1 related to Figures 1 and 2

A Xenograft

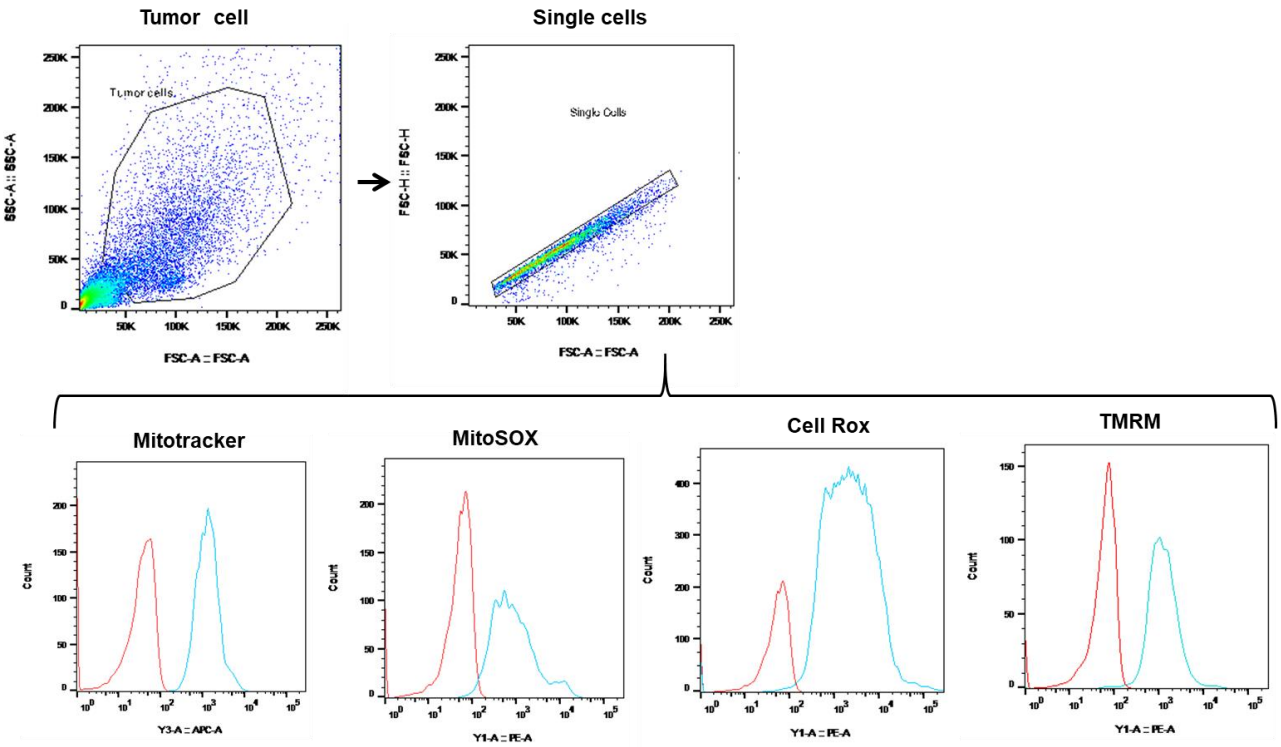

B Allograft

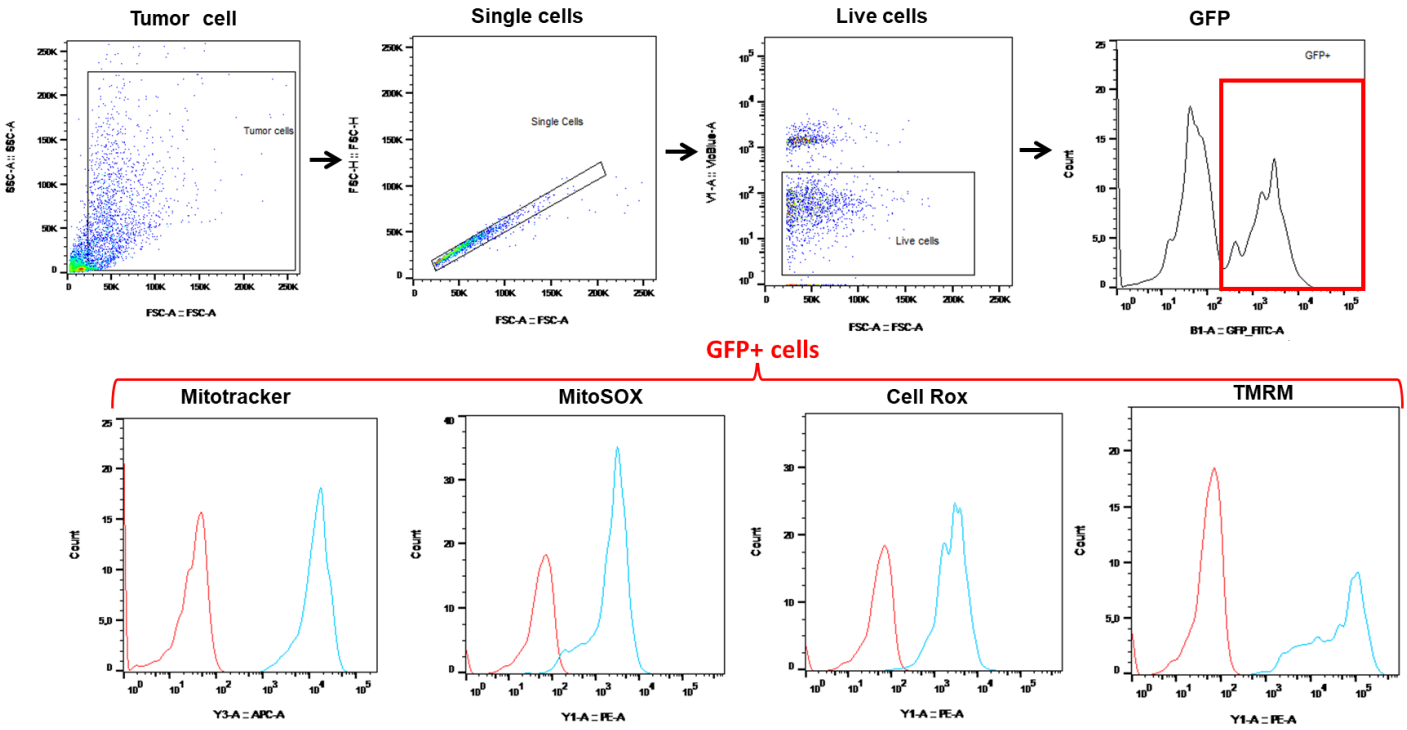

Relative MFI = MFI (stained) / MFI (non stained) Non stained Stained

Supplementary Figure 2 related to Figures 1 and 2

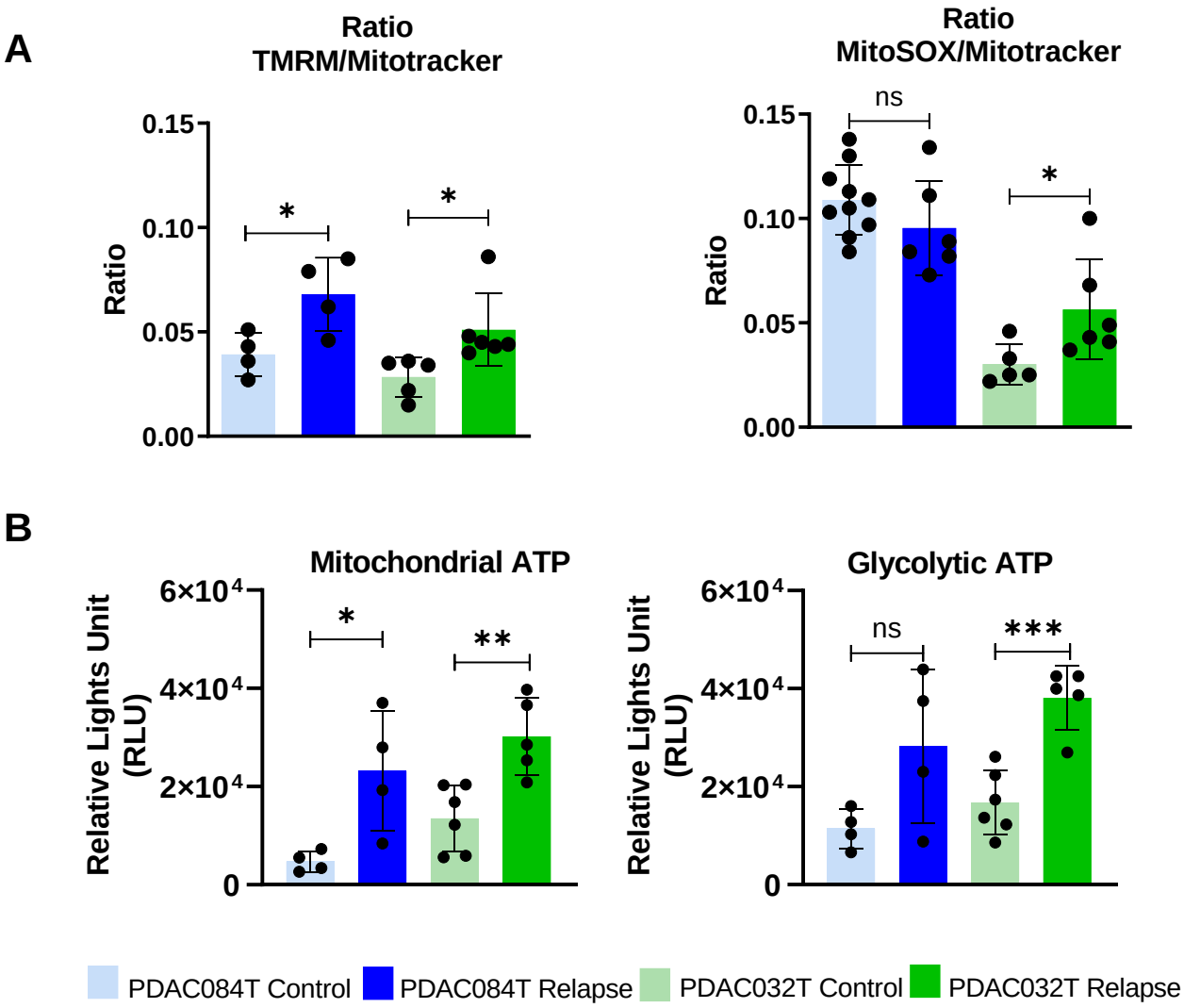

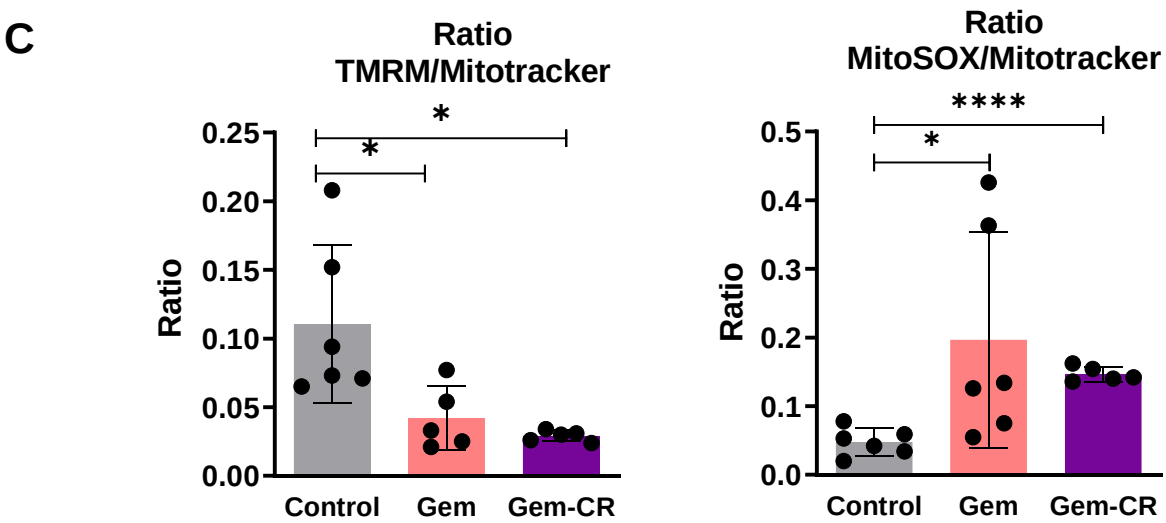

Supplementary Figure 3 related to Figure 1

A PDAC032T

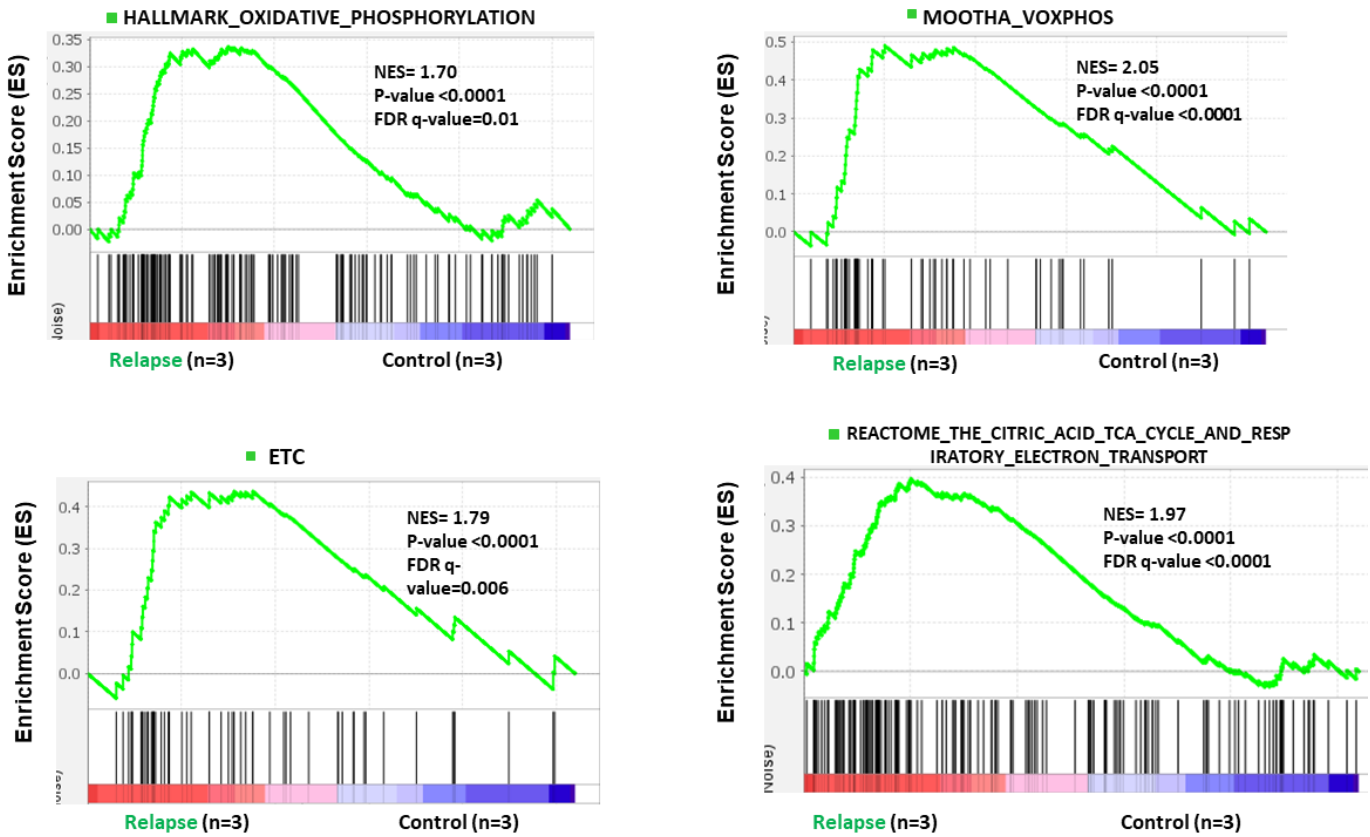

B

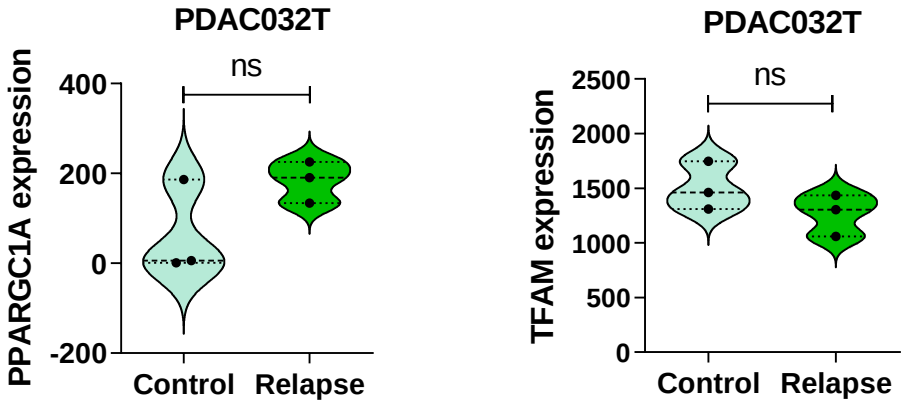

Supplementary Figure 4 related to Figure 3

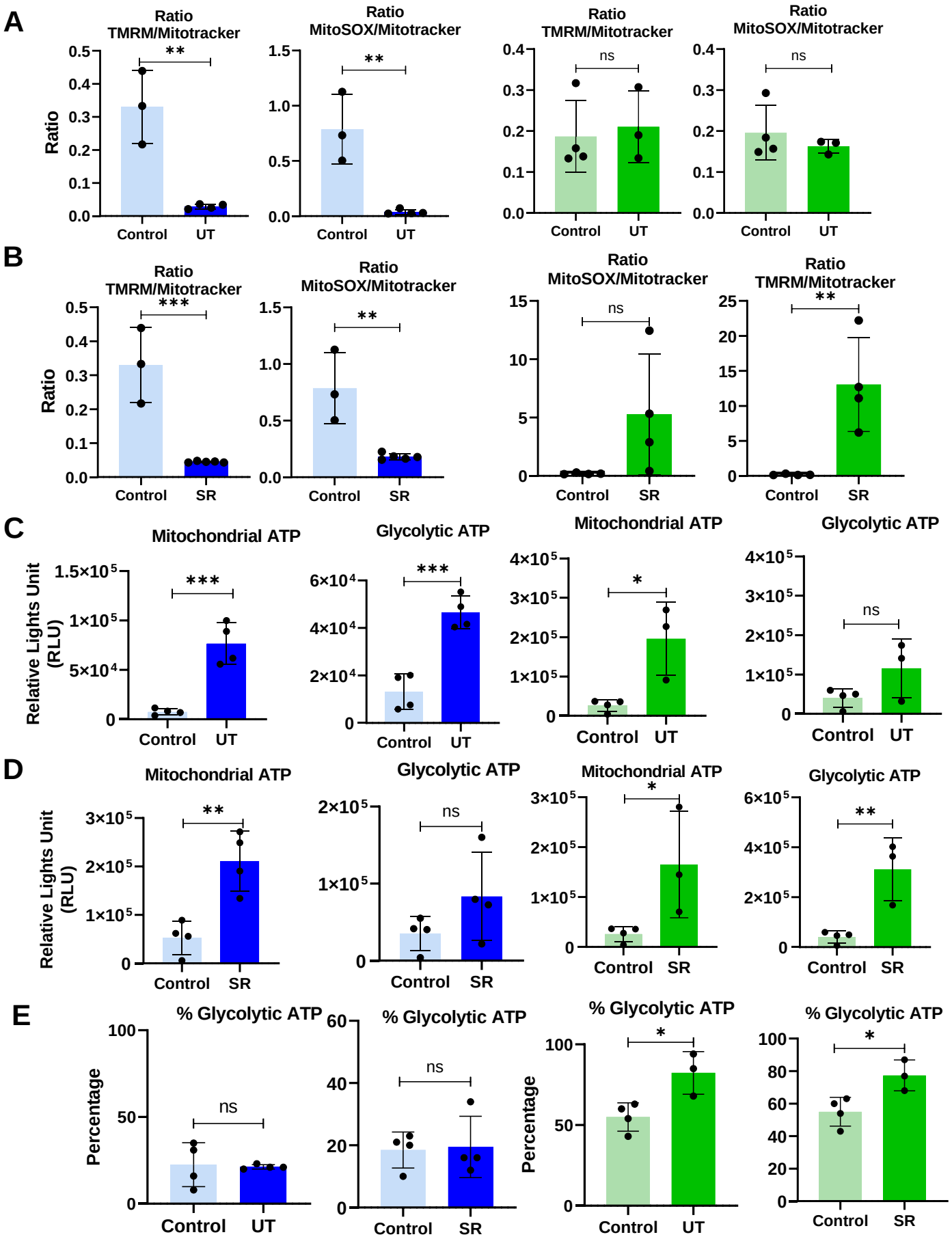

Supplementary Figure 5 related to Figure 3

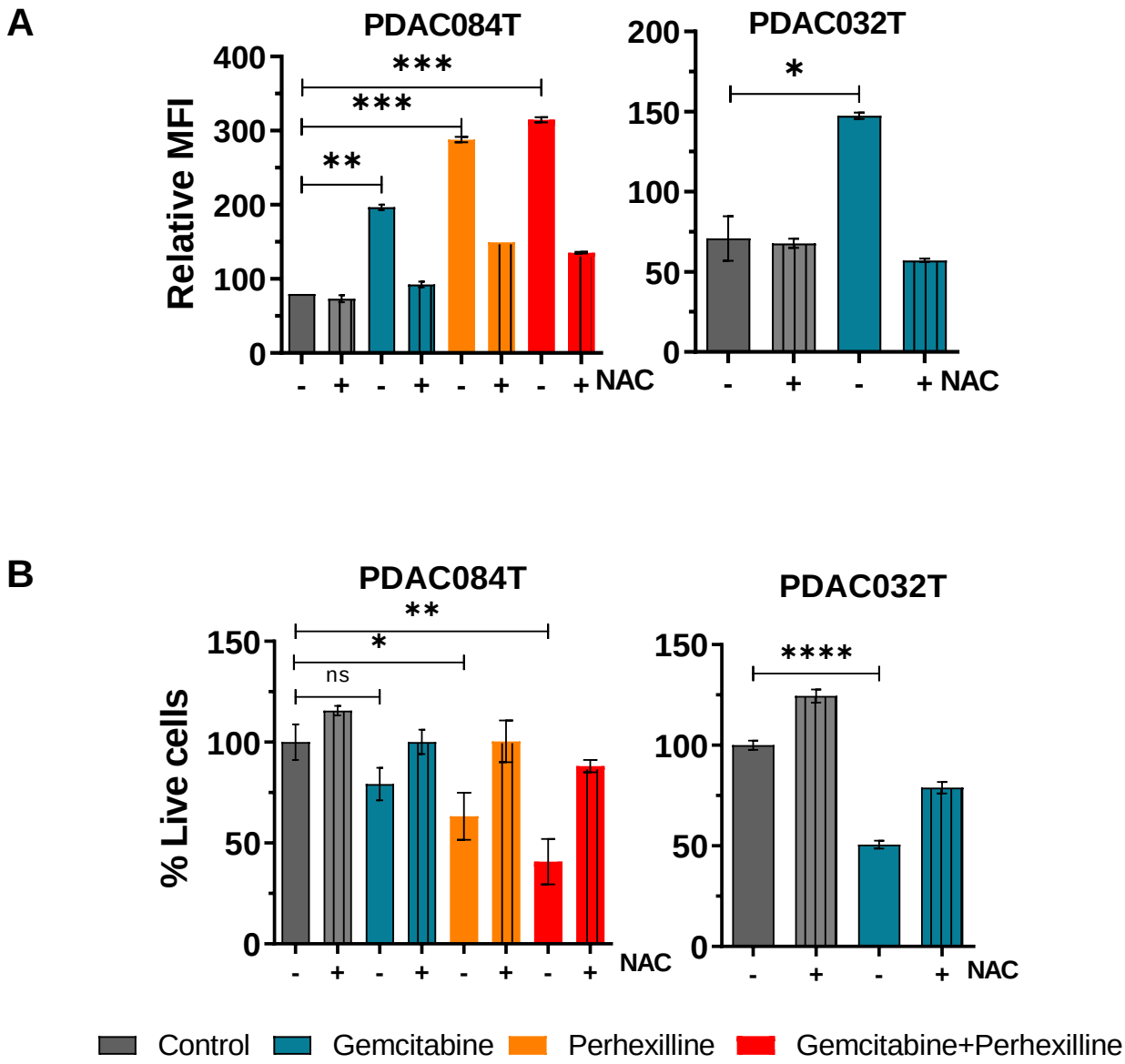

Supplementary Figure 6 related to Figure 4

A

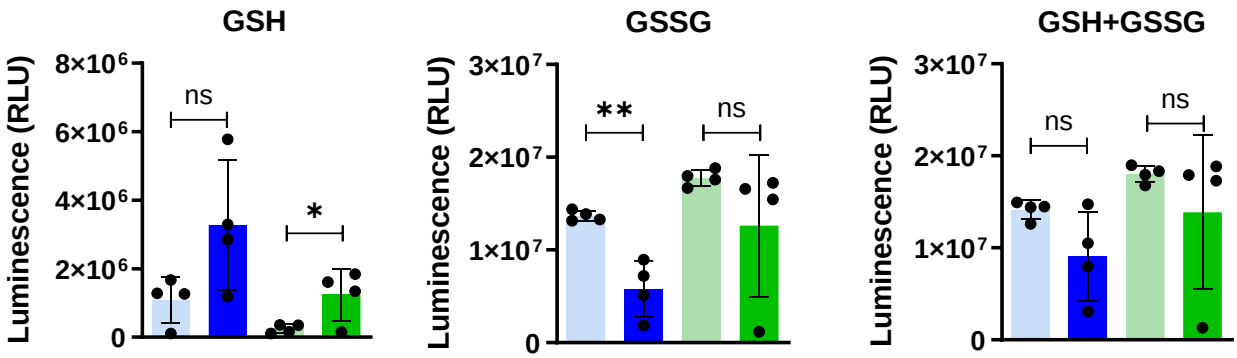

B

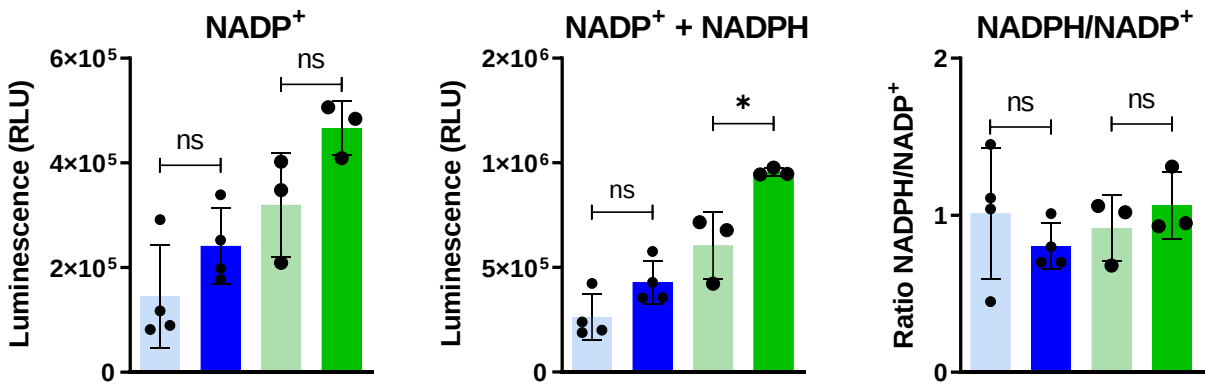

Supplementary Figure 7 related to Figure 5

A PDAC032T

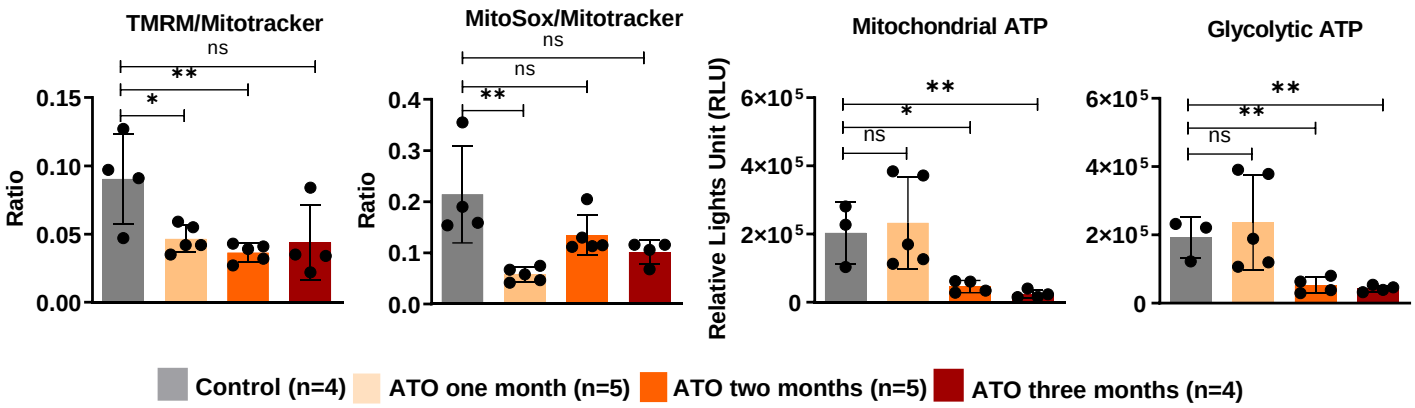

B PDAC084T

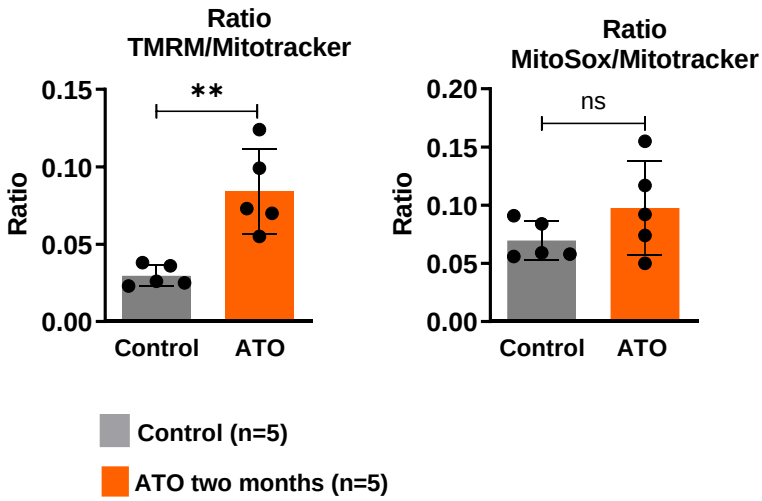
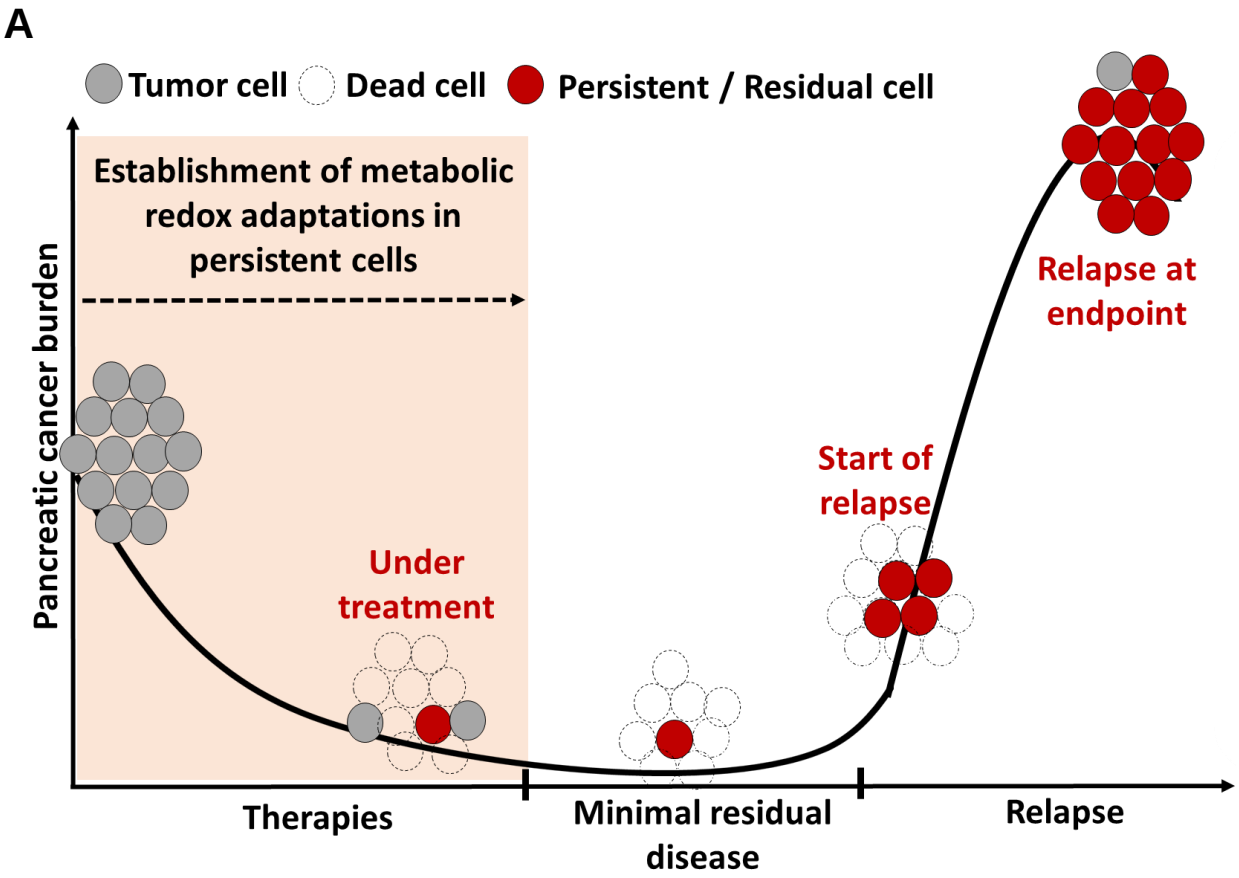
Supplementary Figure 8